RHODES UNIVERSITY

Where leaders learn

Co-crystal Formation of Pharmaceutical and Veterinary Tranquilizer Molecules

Bongeka Naledi Precious Mngwengwe

Dissertation presented in fulfilment of the requirements for the degree of Master of Science

in the Department of Chemistry

Rhodes University

June 2024

Supervisor: Dr V. Smith

Co-supervisor: Prof. R.B Walker

Acknowledgements

I would like to thank my supervisors, Dr Vincent Smith and Prof. Rod Walker. Thank you, Dr Smith, for your committed supervision, support, encouragement throughout this journey and your guidance through image preparation and data interpretation. Thank you, Prof. Walker, for trusting me with this research, providing the veterinary tranquilizer API, and encouragement to make this project a success.

I am deeply thankful to my family for their unwavering support, especially my mother, who has always been there for me and listened when I needed to vent. My extended family, your support and kindness throughout my university years have been invaluable.

To my colleagues in the SMALL research group, thank you for your support and encouragement. Your shared knowledge and advice have been appreciated throughout this journey.

To my friends and loved ones, thank you for your endless love, support, and for holding me accountable to complete all my work.

Rhodes University and Sandisa Imbewu for their financial support.

Abstract

Midazolam, a 1,4-benzodiazepine derivative is commonly used to treat anxiety, insomnia and may be used as a sedative in anaesthesia as it has calming, anti-convulsant and muscle relaxant properties. Midazolam has a rapid onset but a short duration of action resulting in fewer adverse effects. Midazolam also has the potential to form insoluble crystalline precipitates in pharmaceutical dosage forms such as syrups and solutions, which is a challenge in formulation and process development activities. The primary goal of this research was to prepare multicomponent crystals of midazolam free base, specifically targeting interactions with coformers structurally similar to methyl paraben. Key preparation techniques included neat grinding, liquid-assisted grinding, and slow evaporation. The resulting solid forms were characterized using Fourier Transform Infrared Spectroscopy (FTIR), Differential Scanning Calorimetry (DSC), and powder X-Ray Diffraction (PXRD). In addition, Single-Crystal X-Ray Diffraction (SCXRD) was used to elucidate detailed structural information on the novel multicomponent crystals formed.

Successful preparation of midazolam free base from the hydrochloride salt was confirmed through FTIR, DSC, and PXRD analysis. Different co-crystals and salts of midazolam with coformers such as salicylic acid (SA), benzoic acid (BA), 3-hydroxybenzoic acid (3-HBA) and p-aminobenzoic acid (PABA) were synthesized and characterized. The structure of the single crystal obtained from a veterinary tranquilizer solution was solved and found to be a salt that had formed between midazolam free base, midazolam HCl, and methyl paraben. This finding inspired further investigation of similar multicomponent crystals of midazolam and methyl paraben analogues.

This study demonstrated the effectiveness of both mechanochemical and slow evaporation methods for the preparation of multicomponent crystals. PXRD and DSC provided insights into the stability and purity of the crystals that had formed and the differences in melting points and PXRD patterns were particularly important in this regard. Differences in FTIR spectra were used to distinguish between different solid forms and to confirm the successful formation of new solid forms. Extensive searches in the Cambridge Structural Database (CSD) confirmed that the multicomponent crystals of midazolam, such as MDZ·SA, MDZ·BA, MDZ·3-HBA, and MDZ·PABA, had not previously been reported, highlighting the novelty of these findings.

The research successfully isolated and characterized several novel multicomponent crystals of midazolam, demonstrating the potential of mechanochemistry and solvent evaporation techniques in the development of pharmaceutical and veterinary medicinal applications. These findings contribute to the understanding of cocrystal formation and provide a foundation

for future studies in which the stability and efficacy of midazolam-based formulations can be evaluated.

Table of Contents

Chapter 1: Introduction

1.1 Supramolecular Chemistry

In 1894 Emil Fischer first suggested that an enzyme could interact with a substrate in a similar manner as a key interacts with a lock.[1] The two cornerstones of supramolecular chemistry, which would later become a distinct field in its own right, are reflected in this simple lock and key mechanism approach in which molecular recognition and supramolecular function are crucial. Given that the geometry and non-covalent interactions between interacting partners are compatible, molecular recognition is evident in the lock and key model. Moreover, these highly specific interactions often result in the development of beneficial supramolecular function.[1-3.]

Desiraju[1] suggested supramolecular chemistry, a term that was introduced by Jean-Marie Lehn in 1969, for the study of inclusion compounds and cryptands. The work undertaken by the 1987 Nobel prize recipient Charles Pedersen, Jean Marie Lehn and Donald Cram led to the establishment of supramolecular chemistry as an independent discipline.[4] Lehn defined supramolecular chemistry as “chemistry beyond the molecule” and “the chemistry of the intermolecular bond” suggesting that supramolecular compounds are made by linking molecules with noncovalent intermolecular interactions. Put simply, it is the study of non-covalent interactions between atoms, ions, and/or molecules.[1,4,5.]

1.2 Crystal Engineering

Crystal engineering is comprehensively defined as “the understanding of intermolecular interactions in the context of crystal packing and in the application of such understanding in the design of new solids with specific physical and chemical properties".[6] It is knowledge-based design and synthesis of predictable and controllable supramolecular entities with specific pre-defined properties. The rules of supramolecular valence, or more specifically the chemistry and geometry of intermolecular interactions, which serves as the supramolecular cement influences the supramolecular structure formed. Thus, if molecules are the supramolecular counterparts of crystals, crystal engineering is the supramolecular equivalent of organic synthesis.[6]

Supramolecular synthons are “*kinetically*” defined structural units that express the essential characteristics of a crystal structure and capture the essence of crystals, in terms of molecular recognition. Synthons are comprised of molecular fragments and the supramolecular connections between fragments such as hydrogen bonds, for example and any other directional interactions. An important tenet of synthon theory is that the supramolecular synthon is a reasonable approximation of the entire crystal despite the inherent and necessary

simplifications required in its definition.[7] Several supramolecular synthons are depicted in Figure 1.1, many other synthons exist beyond those shown here.

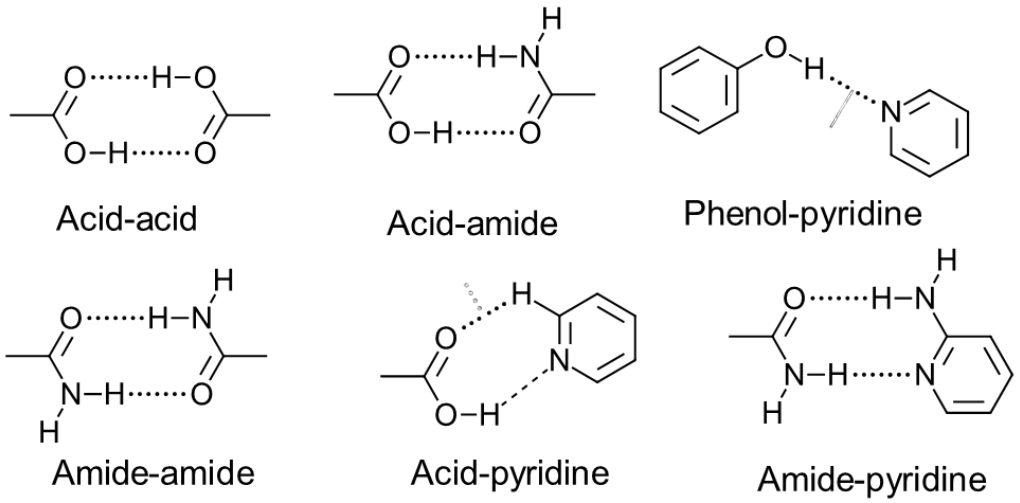

Figure 1.1 - Representative supramolecular synthons adapted from Desiraju.[7]

Active pharmaceutical ingredients (API is used to indicate one or many) of limited aqueous solubility are commonly found in the research and development portfolios of discovery focused, pharmaceutical companies. These API present a multitude of challenges in pharmaceutical development activities and include but are not limited to slow dissolution rates in biological fluids, insufficient and inconsistent systemic exposure with the result of inadequate efficacy in patients, particularly following oral administration.[8] Due to the advancement in the pharmaceutical sciences, numerous strategies have been developed to address the potential issues resulting when dealing with compounds that exhibit low aqueous solubility. Crystal engineering approaches that have the potential to be applied to a wide range of crystalline materials can be used to improve the solubility, dissolution rate and subsequent bioavailability of many poorly water-soluble API.[8]

Improving the physiochemical properties and stability of several benzodiazepine compounds is the primary goal in this study, exploring the molecular behavior and adding to the body of knowledge that will eventually explain how molecules collectively, form specific crystal packing arrangements and their alignment. The focus of this work is the preparation of co-crystals and salts of midazolam free base.

1.3 Solid forms

Many organic and inorganic compounds exist in different solid forms such as hydrates and solvates. A schematic representation of different solid forms is depicted in Figure 1.2. McCrone states that polymorphs are solid crystalline phases of a specific compound that occur due to the possibility of at least two different arrangements of that compound in the solid state,[9] and therefore correlates different molecular arrangements and crystal forms. The term polymorph

does not include amorphous phases, hydrates and solvates, since they do not have the same chemical composition.[9,10]

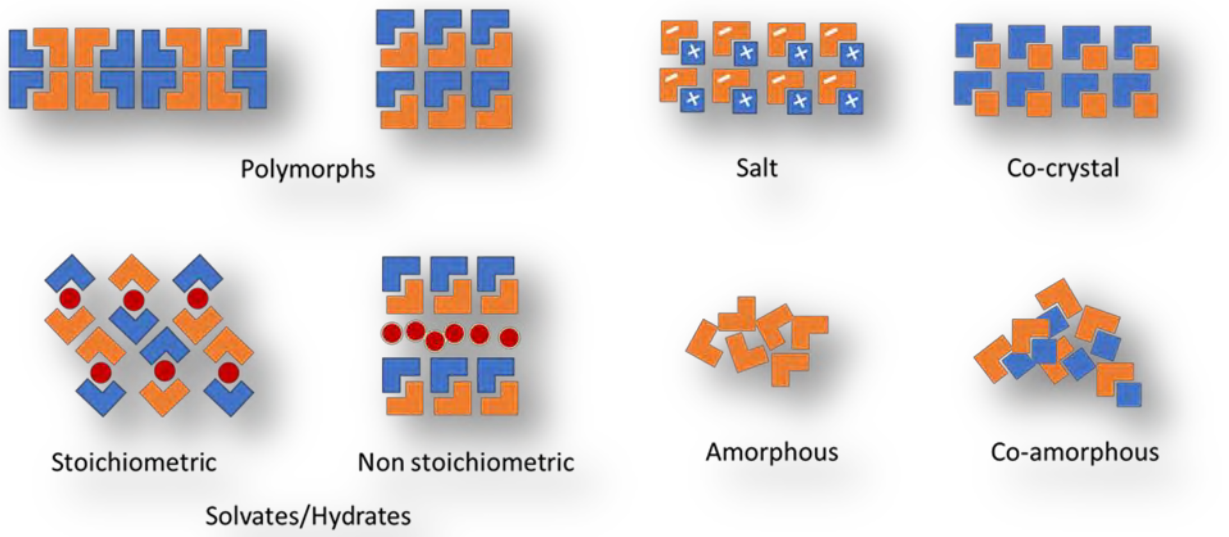

Figure 1.2 - Graphic representation of different solid types of solid forms adapted from Maste et al.[10]

Why any molecule would crystallize in more than one form, particularly since molecular recognition is such a finely balanced process necessitating the minimization of free energy, is highly relevant. One of the most compelling justifications for this phenomenon is that prior to the thermodynamically stable crystal form emerging, the form that emerges first is usually the kinetically stable form.[7]

Since different crystal structures will exhibit different inter- and intramolecular interactions including hydrogen bonds and van der Waal's interactions, different polymorph forms will exhibit different free energies and consequently different physicochemical properties such as solubility, chemical stability, and melting point amongst others, in the solid state.[10] Therefore, the crystal form of a solid compound under development is a crucial quality attribute (CQA) to be monitored. Solvates, are of importance as they reveal the manner in which solvent molecules are incorporated into a crystal lattice in a stoichiometric or non-stoichiometric proportions. Similarly, hydrates, in which water serves as the solvent, are of relevance due to the omnipresence of water.[10]

In the development of solid-state pharmaceutical products, polymorph considerations are addressed after general considerations such as salt or co-crystal formation are investigated. When a compound is weakly acidic or basic, it is generally converted to a salt with a suitable

conjugate base or acid, which can then be crystallized. During this process polymorphic or solvated forms may result.[10]

1.3.1 Co-crystals

In an article titled 'Polymorphs, Salts, and Co-Crystals: What's in a Name?' published in 2012, the forty-six co-authors defined co-crystals as solids crystalline single-phase materials composed of two or more different molecular and/or ionic compounds typically in a stoichiometric ratio.[11] It is noteworthy that this definition is more inclusive than the definition in the draft guidance document issued by the Food and Drug Administration (FDA) in which co-crystals are defined as "solids that are crystalline materials composed of two or more molecules in the same crystal lattice" and, includes solvates, and excludes inclusion complexes and solid solutions.[11]

There is no definition that enables precise categorization of every single crystalline solid since there is insufficient experimental data to draw conclusive comparisons between two types of solids.[11] However, certain crystalline solids consist of a variety of components that even genuine attempts at comprehensively defining it in a legal and scientifically clear manner, fail. As a result, for the purposes of this dissertation, crystalline solids that compromise two or more organic compounds used in specific stoichiometric proportions shall be referred to as a **multicomponent crystal** (MCC). If one of the molecules in the crystal structure is water or solvent, it will then be referred to as a hydrate or solvate, respectively.[11] The MCC will be considered a co-crystal if one or more of the reactants that are present in the crystal are liquids at reaction temperature or when a liquid serves as both a reactant and a solvent at the same time.[11] Thus, if the components of the MCC are ionised, the MCC is then referred to as a salt.

If a co-crystal is prepared from solution, it is preferable that the compounds have comparable solubilities in the solvent selected for this purpose as poorly soluble compounds are likely to precipitate, leaving the more soluble reactant in solution, if the solubilities of each compound in the solvent are vastly different.[11] It may also be useful to include a co-crystal former that exhibits polymorphism as such compounds have displayed an ability to exist in different packing arrangements and different solid-state structures. This suggests that since the molecule is not thermodynamically trapped, into a particular packing mode due to structural flexibility, it is more likely to coexist with other molecules within a multicomponent solid.[11]

1.3.2 Salts

Co-crystals, as multi-component solids, contain only neutral species whereas salts contain anionic and cationic species usually due to proton transfer between the acid and the base.

Proton transfer is difficult to establish experimentally, especially partial proton transfer. Under incomplete transfer, it is difficult to identify the category of multi-component solid that would best describe the compound.[11] Consequently, definitions and nomenclature aside, it is arguably more critical to determine whether co-crystals and salts show any noticeable differences in terms of their synthesis, properties, and /or behavior. If the purpose is to synthesize a multi-component solid with a specific chemical composition or stoichiometry, co-crystals rather than salts offer significant advantages in respect of predictability.[11]

1.3.3 Pharmaceutical Co-crystals

Typically, pharmaceutical products contain an API in combination with inactive ingredients or excipients, to make a dosage form that is subsequently packaged for sale. Formulations are designed to ensure that quality, safety, and efficacy can be assured, and patient adherence is facilitated through aesthetic appeal.[12] The majority of API are solids and crystalline materials that are preferred due to the relative simplicity of isolation and purification.[12] Poor solubility and the presence of one or more crystalline forms of an API are the main issues that may occur when using crystalline solids. Polymorphic forms, salts and stoichiometric solvates have historically been the only crystalline forms of an API that have received regulatory approval. This was again highlighted in 2016 when the FDA revised its guidance document on co-crystals of API.[11,12]

Pharmaceutical co-crystals are defined as a subset of a broader group of multicomponent crystals that include salts, solvates, clathrates, inclusion crystals and hydrates.[12] Solvates, and pharmaceutical co-crystals are in a supramolecular context similar since at least two components of the crystal interact by hydrogen bonding and perhaps other non-covalent interactions rather than through ion-pairing. Alternatively, pharmaceutical co-crystals may also be defined as multicomponent molecular crystals formed by the co-crystallization of an API with organic molecules that have a low molecular weight, also known as coformers.[13]

When comparing pharmaceutical co-crystals to the parent API they may exhibit superior physicochemical properties such as solubility for example. Many API exhibit poor aqueous solubility which can fortunately be altered by one of several economical and simple routes of which co-crystallization, is one. There is an opportunity to identify multiple potential organic co-crystal forms for a particular API because of the availability of a vast number of different potentially useful organic coformers.[11-13]

Approximately 80% of all compounds now under development, when classified according to the Biopharmaceutical Classification System (BCS), fall into BCS Class II or IV. The BCS system classifies compounds according to their aqueous solubility and membrane

permeability. The API that falls into BCS Class II and Class IV exhibit poor aqueous solubility with Class II compounds exhibiting high permeability and Class IV compounds exhibit poor permeability. To solve solubility concerns, formulation scientists frequently use approaches such as micronization, encapsulation, solid dispersion, salt, and amorphous mixture formations. However, these approaches exhibit inherent disadvantages in terms of ease of manufacture and potential instability. Pharmaceutical co-crystals have proved useful in addressing the solubility concerns associated with BCS Class II and IV drugs. Furthermore, by selecting an appropriate coformer, several solid-state challenges such as solubility, chemical stability, hygroscopicity, melting point, mechanical and flow problems can be modified.[11] A schematic representation of the influence of pharmaceutical co-crystals on drug properties and development is depicted in Figure 1.3.

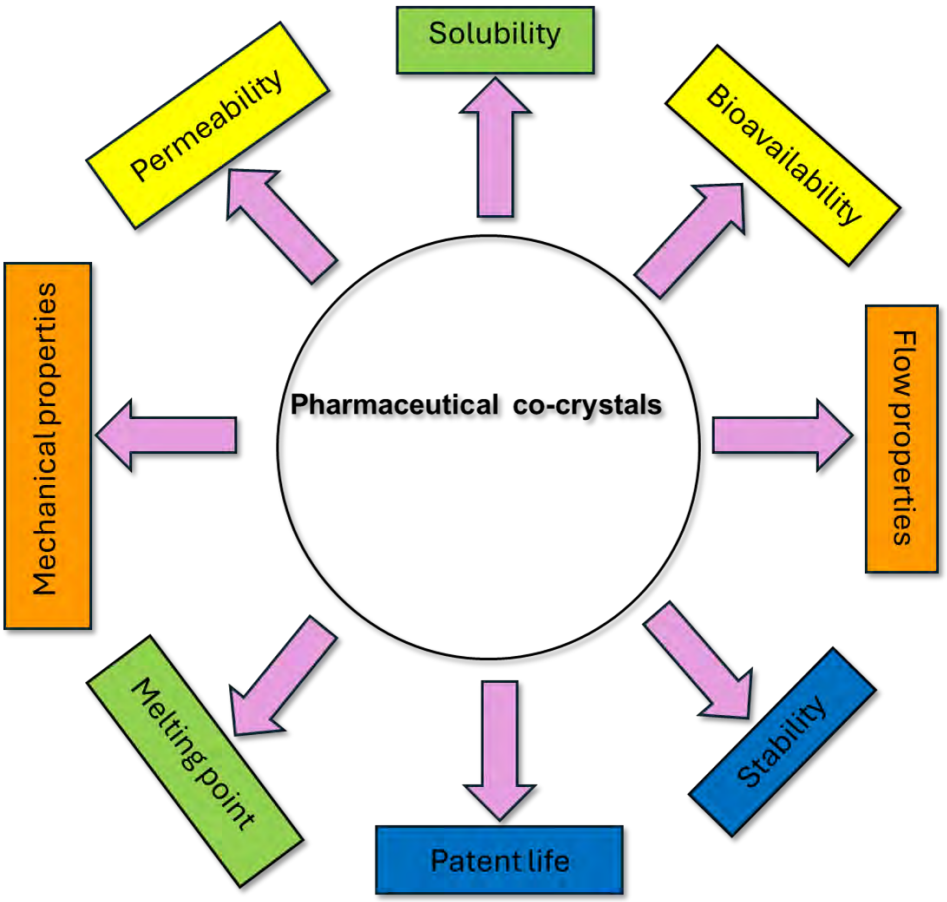

Figure 1.3 - Influence of pharmaceutical co-crystals on API properties and product development activities adapted from Aakeröy et al.[11]

1.4 Coformer Selection

A critical factor in co-crystal design and screening is the identification and selection of a library of complimentary coformers for a specific API molecule. In the context of pharmaceutical co-crystals, an appropriate coformer should be safe enough to be used in a pharmaceutical product and the crystal coformer may be an excipient or another API.[15] A list of compounds

that may be used as prospective coformers for pharmaceutical co-crystals has been documented and maintained by FDA. The coformer should ideally be listed on the US FDA list titled “Everything added to food in the United States” (EAFUS) which contains more than 3000 compounds that are acceptable as additives or are listed and approved on the Generally Regarded as Safe (GRAS) list. It stands to reason that coformers must therefore be non-toxic and exhibit limited or no side effects.[14,15]

Knowledge based and experimental methods are primarily used for coformer selection. The hit and trial approach where several coformers are used for an API is expensive and time consuming since the structure of any co-crystals formed must be characterized using a number of different and sometimes costly, techniques. Researchers have used a variety of knowledge-based methods for the selection of suitable coformers and screening of co-crystals, which include hydrogen-bonding propensity, synthon engineering, supramolecular compatibility from the Cambridge Structural Database (CSD), p*K*a rule, Lattice energy calculations, Hansen solubility parameter determination, the conductor-like screening model for real solvents, and thermal analysis.[14,16]

1.4.1 Hydrogen bonding propensity

Nanda *et al*.[14] state that for co-crystals, the API and coformer(s) interact with each other by non-covalent interactions that include hydrogen bonding and van der Waal’s forces. Of these, hydrogen bonding between the API and the coformer is essential for the formation of co-crystals.[14] Margaret C. Etter[17] in an article titled, ‘Hydrogen Bonds as Design Elements in Organic Chemistry,’ described a graph-set notation that has been used primarily as a motif for labelling hydrogen bonding and proposed three rules for the prediction of preferable bond formation *viz.,* every hydrogen molecule that is acidic in nature will be present in bond formation, all hydrogen bond acceptors will be used when hydrogen bond donors are available, and the best hydrogen bond donor and the best hydrogen bond acceptor will preferentially form a hydrogen bond with each another.[17] These rules reflect the energetically favored types of intermolecular association possible. Assigning a value between 0 and 1 and noting that higher values reflect the formation of a hydrogen bond, was the approach used to analyze the quantitative measurement of hydrogen bond formation between the donor and acceptor functional groups in indomethacin and nicotinamide.[17,18]

1.4.2 Synthon Engineering approach

The synthon approach is one in which coformers and API form supramolecules through specific molecular fragments within a cocrystal, has been reported.[6] According to this approach, the functional groups present in both the API and coformer compound are critical for the formation of co-crystals.[6] Synthons, which are the basic structural constituents

associated with noncovalent bonding are present in supermolecules. There are two types of supramolecular synthons *viz.,* supramolecular homo-synthons and supramolecular hetero-synthons. In contrast to supramolecular hetero-synthons, which are formed by different groups such as carboxylic acid-amide hetero-synthons, supramolecular homo-synthons are comprised of the same functional groups that are present in both the API and coformer. In general, supramolecular hetero-synthons are preferred to homo-synthons for example, acid-amide and acid-pyridine hetero-synthons are more frequently formed than carboxylic acid and amide dimers.[14]

1.4.3 Cambridge Structural Database

The Cambridge Structural Database (CSD) is a database used to store information relating to the crystal structure of molecules and is a verified tool for co-crystal screening, since it lists coformers that can be used with a specific API depending on the availability of a suitable supramolecular hetero-synthon. The CSD is a well curated and frequently updated resource with over 50 000 new structures uploaded on an annual basis. Statistical analysis of packing motifs provides information about the common functional groups present in co-crystals and this information permits researchers to use virtual screening techniques to identify suitable co-crystal forming pairs so that co-crystals can be designed using molecular modeling, reducing research time and experimental costs.[14,19]

1.4.4 p*K*a Rule

To predict and, in turn, control the assembly of a multicomponent solid form, it is essential to determine whether proton transfer will occur in solution. The basicity and acidity of functional groups involved in hydrogen bonding will impact the transfer process and the difference between the pKa of the acidic and basic functional groups can be determined using equation 1.1.

$$\Delta pK_a = [pK_a\,(\text{base}) - pK_a\,(\text{acid})] \qquad \text{Equation 1.1}$$

Generally, proton transfer will occur from an acid to a base if the difference between the p*K*a is > 2 or 3. The formation of co-crystals and salts is likely if values > 2 or 3 are calculated. A total of 6465 co-crystals from the CSD were studied to develop and verify the Δp*K*a rule. This study also revealed that a linear relationship exists between p*K*a and the likelihood of proton transfer between an acid-base pair.[20] A non-ionized complex should form when the Δp*K*a is -1 and an ionized complex is likely to form when Δp*K*a is -4. The possibility of forming an ionized complex increases by 17% with each unit increase in Δp*K*a from 10% at Δp*K*a = -1 to 95% at Δp*K*a = 4. The possibility of co-crystal and salt formation can be evaluated by calculating the Δp*K*a. This method is simple, less time consuming and less costly than actually

preparing co-crystals; however, it does not guarantee co-crystal or salt formation but should rather be considered as a guide.[14,21]

1.4.5 Thermal Analysis

To examine prospective co-crystals of stoichiometric diversity, differential scanning calorimetry (DSC) and hot stage microscopy (HSM) are well-known techniques for solid state form analysis and characterization. These techniques facilitate rapid, solvent-free, and reliable observation. The DSC technique involves heating a physical mixture of two potential cocrystal forming components to a temperature higher than their eutectic points, which involves a melt recrystallization process and, should be observed in DSC profiles generated at a lower heating rate, since it gives the new solid phase time to recrystallize during the solid-solid phase transformation process.[19,22]

Zhou et al.[22] proposed that three endotherms and two exotherms represented co-crystal formation with stoichiometric diversity, two endotherms and one exotherm represents formation of a co-crystal of specific molar ratio, while the presence of a single endotherm suggests no co-crystal formation occurs.[22] It can therefore be inferred that the presence of an exotherm is reflective of co-crystal formation. The use of DSC is not appropriate for compounds that are thermally unstable and volatile as some physical transformations that occur during analysis may lead to ambiguous results. Consequently, the use of hot stage microscopy is necessary to facilitate interpretation of ambiguous results.[22]

Hot stage microscopy technique is also known as the Kofler contact method and when two components are heated, it allows for the visualization of cocrystal formation. The method involves melting one of the co-crystal components (coformer or API) with a higher melting point and letting it solidify.[19] The component with the lower melting point is likewise melted and placed in a contact zone with the other component. The solidified component is then dissolved in the liquid (melted) component creating a mixing zone where the sample is quenched and then recrystallized. The pure components should fall on either side of the mixing zone. The sample is heated once again, until the melting point is reached. The new co-crystal should be located in the mixing zone and will interact differently with polarized light as opposed to the adjacent pure components.[19,22]

1.5 Co-crystal Synthesis

Over the past few years solid state formation chemistry has attracted notable interest due to the advantages associated with the experimental methods used in co-crystal synthesis. The outstanding purity, quality, the high throughput, and rapid processing times are some of the key advantages of these methods. Ultrasound assisted dissolution, supercritical fluid atomization, spray drying, and hot melt extrusion are some of the recently used approaches

for co-crystal formation. Mechanochemical grinding and solution-based methods were used and are reported herein. Solution methods require a suitable solvent to be used for co-crystal preparation. Different solution preparation methods including solvent evaporation, antisolvent addition, and the slurry conversion method may be used. The two types of mechanochemical grinding used are neat grinding (NG) and liquid assisted grinding (LAG).[15,23]

1.5.1 Mechanochemistry

Mechanochemistry is defined by the International Union for Pure and Applied Chemistry (IUPAC) as any "chemical reaction that is induced by the direct absorption of mechanical energy".[24] Over the last 20 years, it has become increasingly clear that this definition falls short as it does not describe the broad reach of modern mechanochemistry adequately. The definition has now been expanded to explicitly include the processes of molecular recognition and self-assembly in the solid state in addition to more conventional organic and inorganic transformations.[11]

Manual grinding using a mortar and pestle is typically sufficient to induce a mechanochemical transformation (of molecular materials). These transformations occur in co-crystal formation, salt formation, and polymorphic changes. Etter *et al*.[25] used this technique to prepare a 1:1 co-crystal of methyladenine and methylthymine to prove that specific molecular recognition may occur in an interaction between two solids during grinding.[11,25] While manual grinding is a straightforward starting point for mechanochemical reactions there are many drawbacks that include the lack of control over the reaction environment, poor reporting of reaction conditions, such as temperature and atmospheric conditions (*e.g.*, humidity or CO_2 content) during experiments, and the duration of the grinding process.[11]

Mechanochemistry, which is not as ubiquitous as solution-based procedures, exhibits a few significant advantages over its more prevalent counterpart such as being more environmentally friendly due to little or no solvent involvement, its limited temperature dependence (in fact, most reactions of this kind are to be performed at room temperature), short reaction periods, and the experimental design is free of solubility considerations and waste handling. These advantages have led to increased interest in the use and application of mechanochemistry.[11,23]

Ball milling can be used in place of manual grinding. There are different designs for electric ball mills and includes laboratory mixer mills and planetary mills that have dominated the co-crystallization research field to date. The co-crystal components are loaded into a cylindrical vessel, also known as a milling jar, together with milling media in the form of balls made of a different material such as stainless steel, zirconia or other materials. The shaker milling assembly is agitated along an axis, and the mechanochemical process occurs because

of the collisions and shear forces produced by the motion of the milling media.[11] The frequency of shaking and time of milling are regulated electronically when using laboratory milling equipment.

Planetary mills are an alternate laboratory milling design in which the cylindrical milling assembly rotates around its own axis in addition to a central axis simultaneously, simulating the motion of planets around the sun. This motion generates significant centrifugal forces on the milling media housed within each milling jar, resulting in sample mixing, shear and crushing forces. The mixer mill is used for sample sizes ranging between 0.01 and 1 g, whereas the planetary mill is used for larger sample sizes ranging between 10 to 100 g.[11,23]

1.5.2 Liquid Assisted Grinding

In the solid-state molecular mobility is reduced, which could reduce the success of co-crystal formation. To overcome this challenge, a small volume of solvent of approximately 0.05 to 0.15 ml is introduced into the milling jar or the mortar and pestle to act as a catalyst while assisting the grinding process.[23,26] This is known as liquid assisted grinding (LAG). The liquid serves only as a catalyst and is depleted during the grinding process. In many instances, LAG is superior to NG and has been used to produce co-crystals that would otherwise be impossible to form by solvent free or solution-based methods. The capacity to accelerate and broaden the scope of mechanochemical crystallization using LAG are well documented in the literature.[11,23,26] For example, Childs *et al*.[27] were able to produce five novel co-crystals of piroxicam with distinct carboxylic acid coformers using LAG after prior attempts using NG failed. In one of these examples, a 1:1 M ratio mixture of piroxicam and adipic acid was ground with no solvent for four minutes and yielded no results. Acetonitrile was added to the mixture and a complete piroxicam-adipic acid co-crystal was produced within two minutes, demonstrating the importance of solvent addition in facilitating co-crystal formation with these compounds.[27]

1.6 Sedatives and Tranquilizers

In veterinary practice, sedatives and tranquilizers play a crucial role when treating companion and wild animals. The use of these medicines as a component of an anaesthetic regimen ensures a range of benefits, including patient calmness, facilitation of intravenous catheterization, provision of analgesia, minimization of anaesthetic requirements, and enables smooth induction to and recovery from anaesthesia. The selection of an appropriate API should be specific for each patient. Due to the species variability and the dosages required, the specific difference(s) between performance of an API as a sedative or a tranquilizer is vague.[28]

An overall feeling of calm is produced by anxiolysis. While reducing anxiety, sedatives

also slow the overall reaction of the body to external stimuli and some, but not all sedatives may also have an analgesic effect. Clinical practice reveals that the manner in which different species react to a specific class of medicine can vary significantly. In addition, exhibiting different effects in different patients within a same species. The terminology reported in different sources of information varies, however; in this dissertation, all medicines are referred to as sedatives since it is known that effects differ with species and dosage used. The sedatives currently used in veterinary medicine fall into different therapeutic classes and are frequently used to induce a state of calm, sedation, possibly analgesia and include but are not limited to phenothiazines, benzodiazepines, opioids, butyrophenones and α_2-adrenergic receptor agonists.[28] This dissertation will focus solely on a selected benzodiazepine compound.

1.6.1 Benzodiazepines

Benzodiazepines are anxiolytic compounds which exhibit a rapid onset and duration of action of several hours to days, depending on the specific molecule used and species being treated. The generalized molecular structure of a benzodiazepine, which is a bicyclic heterocyclic molecule consisting of a benzene ring that is attached to a seven-membered diazepine ring with two nitrogen atoms are characteristic of all benzodiazepines as depicted in Figure 1.4.[28,29] There are different types of benzodiazepines including 1, 2-, 1, 3-, 1, 4-, 1, 5-, and 2, 3-benzodiazepines. The 1, 4-benzodiazepines are commonly used to treat anxiety, insomnia, and for the induction of anaesthesia as they exert calming, anti-convulsant and muscle relaxing activity. The use of benzodiazepines has become prevalent, and they are now widely prescribed. Drowsiness, tolerance, addiction, and withdrawal are common side effects of their use. It is critical to identify selective ligands for the central benzodiazepine receptors that exhibit anxiolytic activity without causing side effects.[29] This dissertation will discuss the 1,4-benzodiazepine, *i.e.*, midazolam in the context of multicomponent crystal formation.

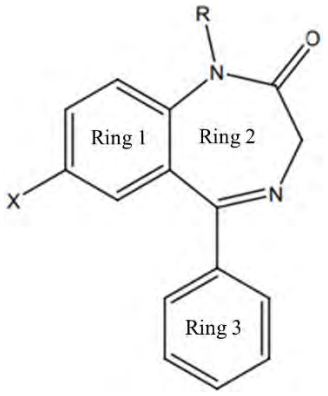

Figure 1.4 - Molecular structure of a typical benzodiazepine adapted from Mohsin et al.[29]

1.6.2 Gamma-aminobutyric Acid

There are specific binding sites for benzodiazepines in the brain, with the limbic system, cerebellum, and central cortex exhibiting the highest density of the receptors.[30] The major inhibitory neurotransmitter in the central nervous system (CNS) is gamma-aminobutyric acid (GABA).[28] GABA exists in dynamic equilibrium with glutamate, the excitatory neurotransmitter. Collectively, the GABA and glutamate systems regulate neuronal excitability. GABA functions through three main receptor subtypes *viz*., GABA-A, GABA-B and GABA-C. The GABA-A and GABA-C receptors mediate rapid effects through a ligand-gated chloride ion channel, whereas GABA-B receptors mediate prolonged effects through G protein-coupled effects on calcium and potassium ion channels.[31] The GABA-benzodiazepine receptor *viz*., GABA-A is comprised of a complex glycoprotein that includes binding sites for different benzodiazepine compounds. The strong anxiolytic effects and pharmacologic bridge suggest this receptor may be involved in the pathophysiology of anxiety in addition to, being important for the treatment of anxiety.[31,32]

The CNS contains a large number of GABA-benzodiazepine receptors, with the density being particularly high in the spinal cord, brainstem, thalamus, cerebellum, and the subcortical regions of the brain including the hippocampus, amygdala, and cortex. The amygdala, hippocampus, and medial prefrontal cortical areas have been implicated, in studies of the neurocircuitry of anxiety, as important way stations promoting anxiety signalling.[31] GABA-benzodiazepines receptors are particularly concentrated in these regions and play a pivotal role in modulating anxiety. GABAergic circuits regulate key excitatory circuits subserved by glutamate and corticotropin-releasing factor in the amygdala. It is plausible that some of the immediate anxiolytic effects of benzodiazepines occur in the amygdala.[31]

Inhibitory functions in the human brain are regulated by GABA receptors. The receptors are protein complexes comprised of five subunits that are pseudo-symmetrically arranged around a chloride selective ion channel. The main GABA receptor is comprised of α_1, β_2, and γ_2 subunits. Benzodiazepines bind to the α and γ interface, resulting in sedative, muscle relaxant, anxiolytic and anticonvulsant activity.[32]

When the GABA-benzodiazepine receptor is activated, there is an increase in influx of chloride ions, which in turn results in membrane hyperpolarization which causes neuronal inhibition. By increasing the frequency of opening of the ion channel, benzodiazepines facilitate the action of GABA rather than independently activating the process. Other psychoactive substances may act at this receptor complex in somewhat different ways and locations. These include barbiturates, anaesthetic steroids, and even alcohol, which also exhibits the same effect of boosting neural inhibition.[4,31]

1.7 Midazolam free base

A breakthrough in the treatment and perspectives of therapy when dealing with mentally ill patients, occurred between 1952 and 1962 during which time, psychotic and psychotropic substances were developed. Benzodiazepines are psychotropic drugs of which diazepam, chlordiazepoxide, and oxazepam possess anxiolytic, sleep-inducing, muscle relaxant and anticonvulsant properties that exhibit different degrees of efficacy. The search for derivatives to produce a medicine suitable for specific cases and symptoms has continued. Nitrazepam and flurazepam are effective sleep inducers, and clonazepam has been shown to exhibit even more anticonvulsant activity than diazepam. Midazolam is mainly used as a sedative before anaesthesia and bromazepam is mainly used as an anxiolytic, however; it also possesses strong sleep-inducing properties.[33,34]

Midazolam free base (Figure 1.5) is an odorless, white crystalline powder and has a molecular weight of 325.78 g/mol. Midazolam hydrochloride is the hydrochloride salt of midazolam and is a white powder with a grainy texture with a molecular weight of 362.23 g/mol. Midazolam is soluble in water, with the pH adjusted to 4, alcohol and slightly soluble in diethyl ether as is midazolam HCl. Similar to other 1, 4-benzodiazepines, midazolam has two benzene rings fused to a seven-membered 1, 4-diazepine ring.[35]

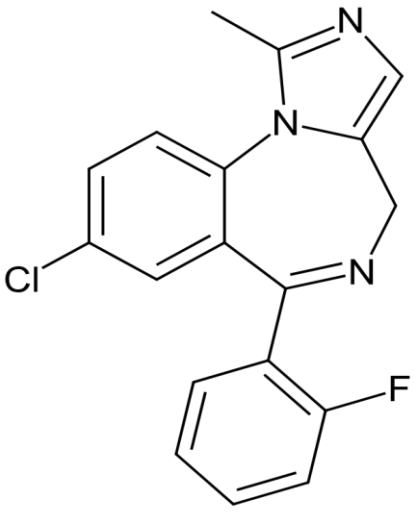

Midazolam, MDZ
M_r = 325.78 gmol^{-1}

Figure 1.5 - The molecular structure of Midazolam free base.

Midazolam exhibits a rapid onset but a short duration of action resulting in fewer adverse effects. Consequently, midazolam is ideal for palliative care as one of four drugs needed to promote better care for dying patients.[31] Midazolam is used in clinical settings as the hydrochloride salt, which is unusual for the benzodiazepines and is essential for the physiochemical properties required for effective anaesthesia. It is interesting to note that the

solubility of midazolam hydrochloride depends on pH and through the use of sodium hydroxide and hydrochloric acid the pH of commercial midazolam hydrochloride products is adjusted to 3.[32,35]

Midazolam binds to the benzodiazepine receptor with a high affinity that lies on the interface of the α and γ subunits of GABA. Benzodiazepines are regarded to be exogenous modulators of the GABA receptor. Comparatively, midazolam binds to the GABA benzodiazepine binding site to a similar extent as clonazepam and lorazepam.[32]

1.8 Project Aims and Objectives

In 2003, Roche Laboratories initiated a voluntary recall of specific lots of midazolam syrup due to the potential presence of a crystalline precipitate of an insoluble complex of midazolam and saccharin. This precipitate compromised the uniformity of the product, which may have led to the administration of either an excessively potent or insufficient dose.[36] This provides additional motivation for investigating midazolam solid forms.

The general aims of this project involves the preparation of multicomponent crystals of midazolam free base and hydrochloride using mechanochemistry and solvent evaporation approaches. The specific objectives are:

1. The preparation of multicomponent solid forms by combining selected API with a preselected set of coformers that are structural analogues of methyl paraben, a preservative.
2. Use neat grinding, liquid assisted grinding, and slow evaporation approaches in the preparation of the multicomponent solid forms of midazolam free base.
3. Bulk characterization of the resulting solid forms using Fourier transform infrared spectroscopy, thermal analysis, and powder X-ray diffraction.
4. Ultimately, characterizing all multicomponent crystals using single-crystal X-ray diffraction.

1.9. References

1 Desiraju G. R., Chemistry beyond the molecule. *Nature*., **2001**, 412, 397–400.

2 Desiraju G. R., Chemistry – The middle kingdom. *Nature*., **2000**, 408, 407–407.

3 Lehn J., Supramolecular chemistry. *Science*., **1993**, 260, 1762–1763.

4 Atwood J. L., Gökel G. W. and Barbour L. J., Eds., *Comprehensive Supramolecular Chemistry II*, Oliver Walter, Oxford, UK, 2nd ed,**2017**.

5 Steed J. W. and Atwood J. L., *Supramolecular Chemistry*, John Wiley & Sons Ltd, West Sussex, UK, 3rd ed, **2022**.

6 Desiraju G. R., in *Stimulating Concepts in Chemistry,* Vögtle, F., Stoddart, J.F., Shibasaki, M., Wiley-VCH, Hoboken, New Jersey, 1st ed, **2000**, p 293-306.

7 Desiraju G. R., Crystal Engineering: A brief overview. *J. Chem. Sci.,* **2010**, 5, 122, 667–675.

8 Blagden N., de Matas M., Gavan P. T. and York P., Crystal engineering of active pharmaceutical ingredients to improve solubility and dissolution rates. *Adv Drug Deliv Rev.*, **2007**, 59, 617–630.

9 Desiraju G. R., Polymorphism: The Same and Not Quite the Same. *Cryst Growth Des.*, **2008**, 8, 3–5.

10 Nanjwade V. K., Manvi F. V., Shamrez A. M., Nanjwade B. K., Maste M. M., New Trends in the Co-crystallization of Active Pharmaceutical Ingredients. *J. Appl. Pharm. Sci.,* **2011**, 1, 1-5.

11 Aakeröy C. B. and Sinha A. S., Eds., *Co-crystals: Preparation, Characterization and Applications.*, Royal Society of Chemistry, **2018**.

12 Almarsson Ö. and Zaworotko M. J., Crystal engineering of the composition of pharmaceutical co-crystals represent a new path to improved medicines? *Chem. Commun.*, **2004**, 1889–1896.

13 Varughese S., Azim Y. and Desiraju G. R., Molecular Complexes of Alprazolam with Carboxylic Acids, Boric Acid, Boronic Acids, and Phenols. Evaluation of Supramolecular Heterosynthons Mediated by a Triazole Ring. *J. Pharm. Sci.*, **2010**, 99, 3743–3753.

14 Kumar S. and Nanda A., Pharmaceutical Cocrystals: An Overview. *Indian J. Pharm. Sci.*, **2017**, 79, 858–871.

15 Duggirala N. K., Perry M. L., Almarsson Ö. and Zaworotko M. J., Pharmaceutical cocrystals: along the path to improved medicines. *Chem. Commun.*, **2016**, 52, 640–655.

16 Thipparaboina R., Kumar D., Chavan R. B., and N. R. Shastri N. R., Multidrug co-crystals: towards the development of effective therapeutic hybrids. *Drug Discov. Today.*, **2016**, 21, 481–490.

17 Etter M. C., Hydrogen Bonds as Design Elements in Organic Chemistry. *J. Phys. Chem.*, **1991**, 95, 4601–4610.

18 Majumder M., Buckton G., Rawlinson-Malone C. F., Williams A. C., Spillman M. J., Pidcock E., and Shankland K., Applications of hydrogen-bond propensity calculations to an indomethacin-nicotinamide (1:1) co-crystal. *CrystEngComm.*, **2013**, 15, 4041–4044.

19 Ross S. A., Lamprou D. A., and Douroumis D., Engineering and manufacturing of pharmaceutical co-crystals: a review of solvent-free manufacturing technologies. *Chem. Commun.*, **2016**, 52, 8772–8786.

20 Cruz-Cabera A. J., Acid-base crystalline complexes and the p*K*a rule. *CrystEngComm.*, 2012, 14, 6362-6365

21 Lemmerer A., Govindraju S., Johnston M., Motloung X., and Savig K. L., Co-crystals and molecular salts of carboxylic acid/pyridine complexes: can p*K*a's predict proton transfer? A case study of nine complexes. *CrystEngComm.*, **2015**, 17, 3591–3595.

22 Zhou Z., Chan H. M., Sung H. H. Y., Tong H. H. Y., and Zheng Y., Identification of New Cocrystal Systems with Stoichiometric Diversity of Salicylic Acid Using Thermal Methods. *Pharm Res.*, **2016**, 33, 1030–1039.

23 Douroumis D., Ross S. A., and Nokhodchi A., Advanced methodologies for cocrystal synthesis. *Adv Drug Deliv Rev.*, **2017**, 117, 178–195.

24 McNaught A. D., and Wilkinson A., *IUPAC compendium of chemical terminology*, Scientific Publications, Oxford, 2nd ed, **2003**.

25 Etter M. C., Choo C. G., and Reutzel S. M., Self-organisation of adenine and thymine in the solid state. *J. Am. Chem. Soc.*, **1993**, 115, 4411–4412.

26 Karimi-Jafari M., Padrela L., Walker G.M., and Croker D.M., Creating Cocrystals: A Review of Pharmaceutical Cocrystal Preparation Routes and Applications. *Cryst. Growth Des.*, **2018**, 18, 6370-6387.

27 Childs S. L., and Hardcastle K. I., Cocrystals of Piroxicam with Carboxylic Acids. *Cryst Growth Des*, **2007**, 7, 1291–1304.

28 Grimm K. A., Lamont L. A., Tranquilli W. J., Greene S. A., and Robertson S. A., *Veterinary Anesthesia and Analgesia: The Fifth Edition of Lumb and Jones*, 5th ed; Wiley Blackwell, **2017**.

29 Mohsin N. ul A., and Qadir M. I., Recent Structure Activity Relationship Studies of 1,4-Benzodiazepines. *Open Chem. J.*, **2015**, 1, 008–012.

30 Crowell-Davis S. L., Murray T. F., and Mattos de Souza Dantas L., *Veterinary Psychopharmacology*, 2nd ed; Wiley Blackwell, **2019**.

31 Roy-Byrne P. P., The GABA-benzodiazepine receptor complex: structure, function, and role in anxiety. *J. Clin. Psychiatry*, **2005**, 66, 14–20.

32 Prommer E., Midazolam: an essential palliative care drug. *Palliat Care Soc Pract*., **2020**, 14, 1–12.

32 Mandrioli R., Mercolini L., and Raggi M., Benzodiazepine Metabolism: An Analytical Perspective. *Curr. Drug. Metab.*, **2008**, 9, 827–844.

33 Enna, S.J., Bluyand, D.B., *xPharm: The Comprehensive Pharmacology Reference*, Elsevier, Amsterdam, **2008**.

34 Buckingham R., *Martindale: The Complete Drug Reference*, 40th ed; Pharmaceutical Press, London, **2020**.

35 Olkkola K. T., and Ahonen J., Midazolam and other benzodiazepines. *Handb Exp Pharmacol.*, **2008**, 182, 335–360.

36 Khalil S.N., Vije H.N., Kee S.S., Farag A., Hanna E., Chuang A.Z., A paediatric trial comparing midazolam/Syrpalta mixture with premixed midazolam syrup (Roche)., *Paediatr. Anaesth.*, **2003**, 13, 205–209.

Chapter 2: Experimental

2.1 Materials

Midazolam HCl was donated by an industry partner. The co-crystal formers (methyl paraben, benzoic acid, salicylic acid, 4-aminobenzoic acid, 4-aminosalicylic acid, 3-hydroxybenzoic acid, 4-hydroxybenzoic acid and 3,4-dihydroxybenzoic acid) were purchased from Sigma Aldrich and used as received. The solvents ethyl acetate, diethyl ether and methanol used for co-crystal preparation are of reagent grade and were obtained from Tag Solvent Products (Pty) Ltd (Gqeberha, Eastern Cape, South Africa) and used as received.

Midazolam free base was prepared from the hydrochloride salt by preparing 100 mmol solutions of sodium hydroxide and midazolam HCl, separately. The solutions were mixed in a beaker to facilitate the precipitation of the midazolam base. The solution was filtered, and the solid midazolam residue was harvested and dried in an oven at 50°C for three hours. The resultant dry powder was characterized using FTIR-ATR, DSC and TGA while the results were compared to published data CUYCAB[1] to confirm that midazolam free base was obtained.

2.2 Co-crystal preparation

Neat (NG) and liquid assisted grinding (LAG) processes were performed using a mechanical ball mill and an agate mortar and pestle. The mechanical ball mill was constructed using a Makita Jigsaw (Makita Corporation, Japan) that had a ball milling capsule fixed to it. The milling media were zinc coated steel balls with a diameter of 4.5 mm, weighing approximately 0.3 g on average. The milling capsule itself was made of stainless steel, measuring 10 mm in diameter, 35 mm in height with a corresponding volume of 2748.89 mm^3. The agate mortar and pestle had an outer diameter of 50 mm, inner diameter of 40 mm and depth of 18 mm.

The API and respective coformer were combined in a 1:1 molar ratio. The first step in co-crystal preparation was neat grinding of the components using the ball mill for at least 20 minutes at a frequency of 16Hz. The resulting product was then characterized using FTIR-ATR, PXRD, and DSC to determine if co-crystallization had occurred.

The LAG experiments were performed in the same way except that 10 µl of solvent was added to the 1:1 mixture of components prior to milling. The solvents used for LAG included methanol and ethyl acetate. For the LAG experiments conducted using a mortar and pestle two drops of solvent were added to the mortar five minutes after commencing grinding, the material was ground for an additional 10 minutes thereafter.

Co-precipitation experiments were undertaken using the slow solvent evaporation method in which the vials containing solutions of dissolved API and coformer were covered with perforated parafilm and left to stand under ambient conditions. The ground material was

dissolved methanol (alternatively ethanol, diethyl ether, or acetic acid) and heated to between 30 and 50 °C depending on boiling point of the solvent. The solutions were filtered at ambient conditions (22 °C, 101.325 kPa) using 0.45 µm nylon syringe filters (Lasec SA (Pty) Ltd, Gqeberha, Eastern Cape, South Africa) that feature a polypropylene over mold housing and then allowed to crystallize at room temperature.

2.3 Attenuated total reflectance - Fourier transform infrared spectroscopy (FTIR-ATR)

FTIR-ATR is a technique used to measure the absorption or transmission of infrared radiation as a function of wavelength, by a sample. Exposure of a material to infrared radiation induces changes in the vibrational energy of the chemical bonds present in a sample and the effect thereof, is monitored. The infrared spectrum exhibits the absorption bands that are associated with vibrations of specific functional groups within a molecule.[2] After grinding or co-precipitation experiments, their spectra were measured for comparison with the starting materials. Significant shifts in the wavenumber of particular bands were used to determine whether co-crystal/salt formation had occurred.

A Perkin Elmer spectrum 100 FTIR (Perkin Elmer, South Africa) with attenuated total reflectance (ATR), which permits sample scanning directly in their solid or liquid form without requiring any additional preparation, was used to generate the spectra. Perkin Elmer spectrum software (v 10.6.2.1159) was used to collect the data. The collection window was 4000 - 400 cm^{-1}, for 32 scans at a scan speed of 0.2 cm/s. The ground material required no further sample preparation and was scanned as is, while crystals were removed from the mother liquor and dried between sheets of qualitative filter paper - grade 3 (Boeco, Hamburg, Germany) prior to scanning.

2.4 Thermal Analysis

Thermal analysis refers to a range of techniques in which the properties of a sample are measured against time or temperature while the sample is heated or cooled at a fixed rate.[3] The thermal analytical techniques used in this study were the differential scanning calorimetry (DSC) and thermogravimetric analysis (TGA).

2.4.1 Differential scanning calorimetry (DSC)

DSC provides quantitative information about exothermic, endothermic and heat capacity of a sample as a function of temperature and time. The DSC has a two-pan configuration *viz*., sample and reference and measures the energy difference(s) between these pans whilst samples are subjected to a controlled temperature heating program. Once the sample undergoes a thermal transition, the difference in temperature between the sample and reference is plotted as heat flow versus temperature and a DSC thermogram is produced with

peaks and/or troughs that illustrate whether an exothermic or endothermic event has occurred.[4]

DSC is used to determine the melting point and other thermal behavior such as recrystallization, decomposition, and polymorphic transitions. All DSC measurements were performed using a TA DSC 250 with Trios software (v5.0.0.44608), all of which were purchased from TA Instruments (Newcastle, USA). The sample masses ranged between 2 to 5 mg, and the samples were placed in aluminum pans and the lids crimped prior to the analysis. The purging gas was nitrogen, set to a flow rate of 50 ml/min, while the system was heated at a rate of 10 K/min.

2.4.2 Thermogravimetric analysis (TGA)

TGA is a quantitative analytical technique that measures the mass of a sample as the temperature is ramped up to 500 °C while the sample is subjected to either constant or fluctuating gas flow. A thermogram which is the graphical representation of the change in mass of sample vs temperature or time plot is produced, once the run is complete. Thermograms represent the thermal and oxidative stability, multicomponent composition, product lifespan, decomposition kinetics, moisture, and volatile content.[5] The thermogravimetric analyzer was operated with the aid of Pyris manager software (v13.1.1.0160), all TGA studies were performed using a Perkin Elmer TGA 4000 (Perkin Elmer, South Africa). Samples (2-5 mg) were heated at 20 K/min in a ceramic crucible whilst purging the system with nitrogen gas at a flow rate of 19.8 ml/min.

2.5 X-Ray Diffraction

2.5.1 Powder X-ray Diffraction (PXRD)

PXRD analysis of a sample provides useful information pertaining to the crystal structure, sample purity, particle size, preferred orientation and in some instance's morphology and phase identification, of a material.[6] When there is a greater propensity for the crystallites in a texture or powder to be orientated more one way than another, or one combination of ways, than all others, this is known as preferred orientation. When a material with a strong cleavage or growth habit is packed into a specimen, the outcome is an example of preferred orientation.[7] One of the advantages of PXRD is that it is non-destructive, and PXRD patterns are unique for every sample, making it possible to identify the presence of new phases.[6] A Bruker D2 phaser 2nd generation (Bruker, Karlsruhe, Germany) equipped with a CuKα radiation source and Lynxeye detector to record PXRD patterns at 30 kV and 10 mA, with radiation of λ = 1.54184 Å wavelength was used. A 2θ range of 5-60º was used with a step size of 0.04º; PSD opening of 4.859º. A steel sample holder with a 25 mm diameter, was filled completely with

each sample prior to analysis. PXRD was used to confirm that the API and coformer had indeed, formed a new phase by comparison to the PXRD pattern of the ground powder of the starting materials and the calculated PXRD pattern of the crystalline material.

2.5.2 Single crystal X-Ray Diffraction (SCXRD)

The most effective method for elucidating a crystal structure is the use of SCXRD. Single-crystal techniques are always guaranteed to be successful in elucidating precise parameters of cell dimensions for structures with fewer than 100 atoms in an asymmetric unit.[8] A 50 µm-MiTeGeN micro loop was used to mount individual crystals, and immersion oil (Type NVH) was used to coat the crystal. The SCXRD data for each crystal was collected using a Bruker D8 venture (Bruker, Karlsruhe, Germany) equipped with Cu and Mo sources. Radiation was generated at 50 kV and 1.4 mA at a wavelength of λ = 0.71073 Å for Mo.

All data collections for single crystals was performed using APEX 4 software (2021.10-0) and to ensure that temperature fluctuations did not affect acquisition of cell dimensions, unit cell data was collected at both ambient (298 ± 2 K) and low temperature (100 ± 2 K). The crystals were cooled using a continuous stream of nitrogen gas set at a flow rate of 20 cm^3/min and delivered with the aid of a Cryostream cooler (Oxford Cryosystems UK), which allowed for the collection of all data at a low temperature of 100 ± 2 K. φ (phi) and ω (omega) scans were monitored and recorded.

Data reduction was conducted using the Bruker software package SAINT.[9] Absorption correction and rectification of other systematic errors were undertaken and executed using SADABS,[10] and the multi-scan method available within APEX4.[11] The structures were solved by direct methods using SHELXT[12] and subsequent refinement was performed SHELXL.[13] The graphical interface X-Seed[14,15] facilitated the use of the SHELX software suite for solving crystal structures via direct methods and refining them through least-squares minimization. Hydrogen atoms were positioned according to riding model constraints. Supplementary information for each structure was prepared using PLATON.[16]

The salt and co-crystal powder patterns were elucidated using the SCXRD data and Mercury[1] (v2020.3.0) software.

POV-Ray[17] was used to generate images in X-seed based on crystal structure models. All diagrams depicting molecular structure and packing were created using POV-Ray.

2.6 References

1 Macrae C. F., Bruno, I. J., Chisholm J. A., Edgington P. R., McCabe P., Pidcock E., Rodriguez-Monge L., Taylor R., Van De Streek, J., Wood, P. A. Mercury CSD 2.0 - New Features for the Visualization and Investigation of Crystal Structures. *Journal of Applied Crystallography*. **2008**, 466–470.

2 Gaffney J. S., Marley N. A., and Jones D. E. Fourier Transform Infrared (FTIR) Spectroscopy in Characterization of Materials, 2nd ed.; Kaufmann E. N., **2012**.

3 Giron D. Applications of Thermal Analysis and Coupled Techniques in Pharmaceutical Industry. *J. Therm. Anal. Calorim*., **2002**, 68, 335-357.

4 Clas S., Dalton C. R., Hancock B. C. Differential Scanning Calorimetry: Applications in Drug Development. *Pharm Sci Technol Today.,* **1999**, *2* (8), 311–320.

5 Saadatkhah N., Carillo Garcia, A., Ackermann, S., Leclerc P., Latifi M., Samih S., Patience G. S., Chaouki J. Experimental Methods in Chemical Engineering: Thermogravimetric Analysis—TGA. *CJCE*., **2020**, 98(1), 34–43.

6 Holder C. F., Schaak R. E. Tutorial on Powder X-Ray Diffraction for Characterizing Nanoscale Materials. *ACS Nano.,* **2019**, *13* (7), 7359–7365.

7 LibreTexts Chemistry, https://chem.libretexts.org/@go/page/17448 (accessed August 2024).

8 Pan Q. Q., Guo, P., Duan, J., Cheng, Q., Li, H. Comparative Crystal Structure Determination of Griseofulvin: Powder X-Ray Diffraction versus Single-Crystal X-Ray Diffraction. *Sci. Bull.,* **2012**, *57* (30), 3867–3871.

9 *SAINT V8.37A*, Bruker AXS Inc.: Madison, WI **2016**.

10 *SADABS*, Bruker AXS, Inc.: Madison, WI **2016**.

11 *APEX4, SAINT, and SADABS*, Bruker AXS, Inc.: Madison, WI **2016**.

12 Sheldrick G.M. SHELXT - Integrated Space-Group and Crystal-Structure Determination. *Acta Crystallogr A.,* **2015**, *71* (1), 3–8.

13 Sheldrick G. M. Crystal Structure Refinement with SHELXL. *Acta Crystallogr C Struct Chem.,* **2015**, *71*, 3–8.

14 Barbour L. J. A Software Tool for Supramolecular Crystallography. *J Supramol Chem.,* **2001**, 1, 189-191.

15 Atwood J. L., Barbour, L. J. Molecular Graphics: From Science to Art. *Cryst Growth Des.,* **2003**, *3* (1), 3–8.

16 Spek A. L. *PLATON* SQUEEZE: A Tool for the Calculation of the Disordered Solvent Contribution to the Calculated Structure Factors. *Acta Crystallogr C Struct Chem.,* **2015**, *71* (1), 9–18.

17 POV-RAY™ for Windows Version 3.7.0.msvc10win64 Copyright © (1996-2013), Persistence of Vision Raytracer PTY. LTD.

Chapter 3: Midazolam Multicomponent Crystals (Salts)

3.1 Introduction

Midazolam hydrochloride (HCl), the salt form of midazolam, is a water-soluble compound known for its rapid onset and short duration of action.[1] Midazolam HCl is favored over midazolam for effective anesthesia, due to its pH-dependent solubility[2,3] It can be administered as a single dose for sedation prior to anesthesia or as a continuous IV infusion to provide prolonged sedation in an intensive care unit (ICU) setting.[1,2]

Midazolam (MDZ) free base was produced from the hydrochloride salt by preparing 100 mmol solutions of sodium hydroxide and midazolam HCl (MDZ·HCl) separately. The two solutions were added to a beaker and on mixing, the midazolam free base immediately precipitated from solution. The reaction occurred under ambient conditions (22 °C, 101.3 kPa) and the solution was filtered to harvest the midazolam residue, which was dried in an oven at 50 °C for 3 hours. During drying, samples were removed every hour and analyzed using TGA to monitor water content. To avoid the risk of chemically decomposing midazolam, the drying process was stopped after the third hour and TGA revealed an insignificant mass loss that could be overlooked. The resultant “dry” powder was further characterized using FTIR, DSC and PXRD and the results compared to literature to confirm that midazolam free base had indeed, been obtained.

Co-crystals/salts were prepared by liquid assisted grinding of midazolam with the coformers listed in Table 3.1, using methanol as the solvent. Two drops of solvent (approximately 10 µl) were added to the mortar, 5 minutes after commencing grinding. The resulting grinds were used for slow evaporation from diethyl ether, methanol or ethanol. Slow evaporation led to the formation of small, colourless crystals of different shapes. Coformers, which yielded co-crystals/salts, are reported herein and listed in the shaded cells contained in Table 3.1.

Table 3.1- Coformers used in the preparation of with MDZ MCC.

Coformers		% Purity	Country of origin
Methyl Paraben	(**MP**)	99	South Africa
4-Aminosalicylic Acid	(**PAS**)	99	India
Salicylic Acid	(**SA**)	99	France
Benzoic Acid	(**BA**)	99	India
4-Aminbenzoic Acid	(**PABA**)	99	Switzerland
3-Hydroxybenzoic Acid	(**3-HBA**)	99	China
4-Hydroxybenzoic Acid	(**4-HBA**)	99	China
3,4-Dihydroxybenzoic Acid	(**3,4-DHBA**)	99	Switzerland

3.2 WPRU1 muticomponent crystal[†]

3.2.1 Introduction

Through an industry partner we received a vial containing an injectable solution of a veterinary tranquilizer. The preparation, which shall be refered to as WPRU1 consists of a highly concentrated aqueous solution of midazolam hydrochloride (50 mg/ml) (MDZ·HCl) and the preservative, methyl paraben (MP). Also present in the ampoule was a single-crystal of an unknown crystalline composition that had formed during storage. The crystal had approximate dimensions of 0.4 cm × 0.15 cm × 0.18 cm. The presence of the crystal contained in the solution, depending on its chemical composition, is likley to deleteriously affect the consistency of the formulation and possibly lead to inconsistent efficacy. Our first objective was to characterize the single crystal and thereafter gain insight into the conditions that led to its formation. This section covers the characterization of the single crystal obtained from the ampoule as well as the preparation and characterisation of other multicomponent crystals obtained from similar starting materials.

Single-crystal X-ray analysis of WPRU1 MCC

As mentioned previously, a solution containing a large single crystal was received, the crystal was cut to size and used for the SCXRD experiment without any further preparation.

Data collection and space group determination

Unit cell parameters, crystal system, space group and single crystal data were collected on a Bruker D8 Venture diffractometer. A preliminary unit cell dimension check reveals that the WPRU1 MCC crystallizes in the triclinic system, in the space group *P* -1.

Structure solution and refinement

The structure for the WPRU1 crystal was solved using SHELXT[4] and refined using SHELXL.[5] Based on well-behaved isotropic temperature factors, all atoms were refined anisotropically, and hydrogen atoms were placed in idealized positions in a riding model. Peaks from the difference Fourier map were used to refine hydrogen atoms associated to heteroatoms. Data collection and refinement parameters are summarized in Table 3.2.

[†] WPRU1 is the code for the industry partner product.

Table 3.2 - Data-collection and refinement parameters for WPRU1 MCC.

Data-collection and refinement parameters	
Formula unit	$(C_{18}H_{13}ClFN_3)(C_{18}H_{14}ClFN_3)(C_8H_8O_3)Cl$
Formula mass (g mol^{-1})	840.13
Crystal system	Triclinic
Space group	*P*-1 (No. 2)
a/Å	8.9741(11)
b/Å	13.1967(16)
c/Å	17.784(2)
α/°	110.707(2)
β/°	92.042(2)
γ/°	96.922(2)
Volume (Å^3)	1948.8(4)
Z	2
D_{calc} (g cm^{-3})	1.432
F (000)	868
μ (MoKα) (mm^{-1})	0.296
Crystal size (mm^3)	0.08 × 0.14 × 0.20
Temperature (K)	100
Range scanned θ (°)	1.2, 27.6
Index ranges	-11: 11 ; -17: 17 ; -23: 23
Total number of reflections collected	67361
Number of unique reflections	9018
Number of reflections with $I > 2\sigma(I)$	7238
Number of least-square parameters	534
R_{int}	0.062
S	1.04
R_1 ($I>2\sigma(I)$)	0.0371
wR_2	0.0881
Weighting scheme parameters	a = 0.0247, b = 1.6829
$(\Delta/\sigma)_{mean}$	0.00
Δρ excursions (e Å^{-3})	-0.28, 0.32

Molecular structure and noncovalent interactions

The asymmetric unit of WPRU1 multicomponent crystal (MCC), as it turns out, contains a molecule of MDZ·HCl, a molecule of MDZ free base and a single molecule of methyl paraben (Figure 3.1 (A)). The protonated MDZ molecule hydrogen bonds to the MDZ free base molecule (MDZH·MDZ) while the methyl paraben hydrogen bonds to the chloride ion via the hydroxyl moiety O(33)-H(4)···Cl(14), see Figure 3.1 (B).

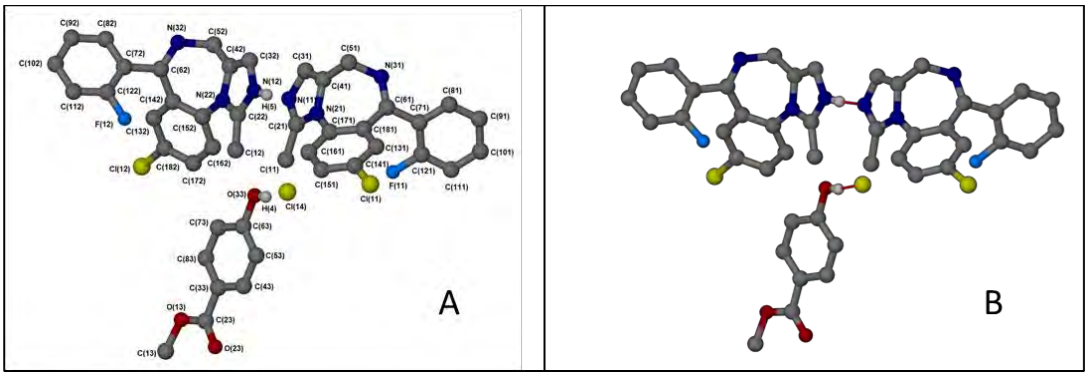

Figure 3.1 (A) – The labelled asymmetric unit of the WPRU1 MCC. (B) Shows the charge assisted hydrogen bond between the two midazolam molecules and the charge assisted interaction between MP and the chloride ion.

The two MDZ molecules interact via an N(12)-H(5)···N(11) hydrogen bond linking both molecules through the imidazole moieties. The protonation of one of the MDZ molecules was determined from single crystal X-ray data. We were able to model a hydrogen atom H(5) covalently attached to the nitrogen atom N(12) from the electron density present in difference Fourier map. The hydrogen bonded complex between the protonated MDZ and MDZ free base carries a positive charge that is charge balanced by the chloride ion present in the structure.

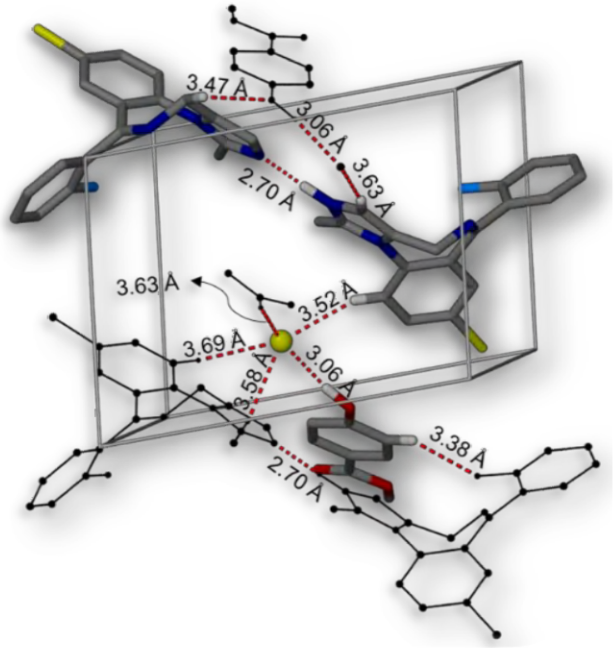

Figure 3.2 – Shown here are some of the noncovalent interactions present in the WPRU1 MCC demonstrating the complexity of all the interactions in the structure.

In addition to the hydrogen bond between the MDZ molecule and the hydrogen bond between the chloride ion and methyl paraben, the structure also contains several other noncovalent interactions. For instance, there are four additional C-H···Cl^- interactions linking three different MDZ molecules to the chloride ion. There are three weak C-H···O interactions and a single C(73)-H(73)···F(12) hydrogen bond between MDZ, and MP as depicted in Figure 3.2. These interaction parameters are reported in Table 3.3.

Table 3.3 – Noncovalent interaction parameters for the WPRU1 MCC.

D-H···A	D···A (Å)	D-H···A (°)	Symmetry Code
O33-H4···Cl14	3.0647(15)	171(2)	.
N12-H5···N11	2.703(2)	176.3(19)	.
C11-H11A···Cl14	3.5823(19)	146.0	1+x,y,z
C32-H32···Cl14	3.6350(18)	167.0	1-x,1-y,1-z
C51-H51A···O33	3.477(2)	154.0	1-x,1-y,1-z
C73-H73···F12	3.382(2)	154.0	-1+x,y,z
C101-H101···O13	3.434(2)	170.0	1+x,1+y,1+z
C102-H102···O23	3.360(3)	140.0	1+x,-1+y,z
C161-H161···Cl14	3.6864(19)	162.0	1+x,y,z
C162-H162···Cl14	3.516(2)	157.0	.

Crystal Packing

The hydrogen bonded units of MDZH·MDZ stack on top of each other forming a centrosymmetric pair, shown as pink and purple molecules in Figure 3.3. The centrosymmetric pairs are translated along the *b* axis forming columns that are stacked parallel to the *b* axis down ([010]) direction. The columns are separated from each other by the hydrogen bonded MP···Cl^- pairs, which are also, centro-symmetrically related.

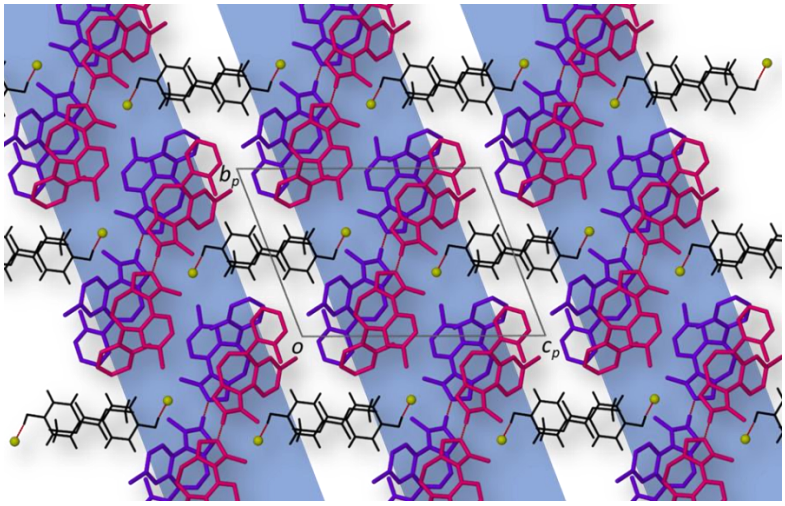

Figure 3.3 – View down the a axis of a single layer of the WPRU1 MCC. A single layer is shown for clarity.

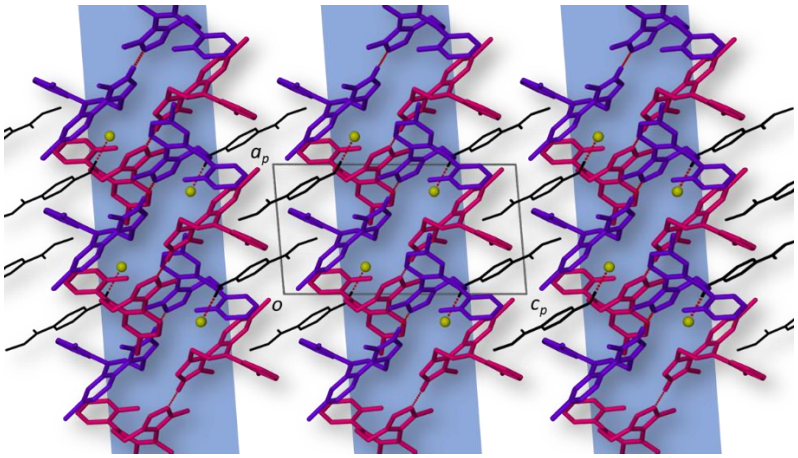

Figure 3.4 – View down the b axis showing the columns of centrosymmetric pairs side-on. A single layer is shown for clarity.

From the view down the *b* axis (Figure 3.4) the centrosymmetric columns of MDZH·MDZ are interdigitated by the MP···Cl^- columns which link consecutive columns of MDZH·MDZ through the hydrogen bonding to the chloride ions and separately the oxygen atoms of the MP molecules.

3.2.2 Bulk characterization

FTIR spectra of WPRU1 and constituent materials

WPRU1 and its component materials were analyzed using FTIR spectroscopy. The spectra of the component materials were used as reference material to characterize the phase of the single-crystal contained in the ampuole. The sprectra are presented below in Figure 3.5.

The MP spectrum shows an ν(O-H) stretching band at 3296 cm^{-1} and a carbonyl ν(C=O) stretching band at 1687 cm^{-1}. These values allign with exisiting literature.[6] The MDZ spectrum is mainly characterized by a weak intensity imine band ν(C=N) at 1680 cm^{-1}, an aromatic ν(C=C) band at 1613 cm^{-1} and two different aryl halide bands ν(Ar-F) at 1139 cm^{-1} and ν(Ar-Cl) at 770 cm^{-1}. The MDZ·HCl spectrum is similar to the MDZ spectrum. MDZ·HCl has a broad ν(N-H) stretch band between 3523-3228 cm^{-1}, and an absence of the imine band. The aromatic ν(C=C) band remains at 1613 cm^{-1}, the aryl halide band for ν(Ar-F) remains at 1139 cm^{-1} while the ν(Ar-Cl) band shifts to 750 cm^{-1}.

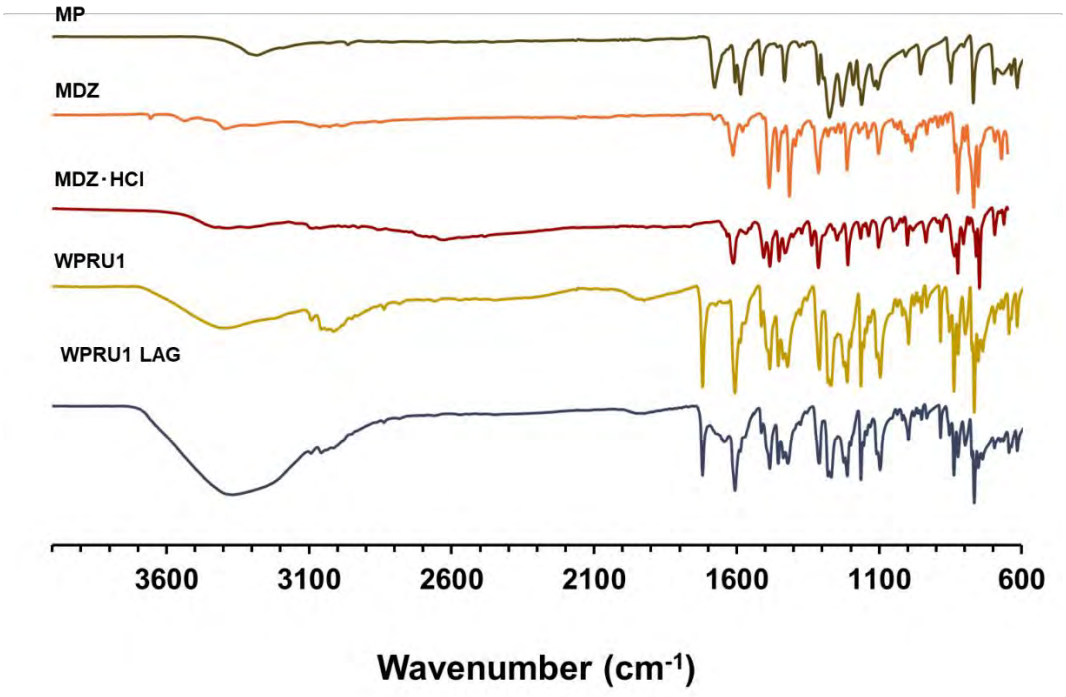

Figure 3.5 – FTIR spectra of methyl paraben (MP), midazolam (MDZ), midazolam HCl (MDZ·HCl), WPRU1, and WPRU1 LAG.

The WPRU1 and WPRU1 LAG spectra are very similar, hence only the WPRU1 spectrum was analyzed; however the vibrational modes for the LAG sample are reported in Table 3.4. The WPRU1 spectrum exhibts a broad ν(O-H) stretching band between 3668-3160 cm^{-1}, this is due to the O-H present in MP. A closer look at the spectrum of WPRU1 shows evidence of the MP carbonyl ν(C=O) at 1720 cm^{-1} shifting from 1677 cm^{-1} due to an O-H···Cl hydrogen bond interaction. Moreover, the weak intensity ν(C=N) band shifts to 1674 cm^{-1} while

the aromatic ν(C=C) band shifts to 1606 cm^{-1} due to the hydrogen bonding between MDZ and MDZ·HCl. A new broad ν(O-H) stretching band centered at 1928 cm^{-1} further indicates the hydrogen bonding effect (see structure Figure 3.1). A summary of the the vibrational modes of the multicomponent crystal is listed in Table 3.4.

Table 3.4 – Vibrational modes for WPRU1 and its components materials.

Vibrational Modes	MDZ (cm^{-1})	MDZ·HCl (cm^{-1})	MP (cm^{-1})	WPRU1 LAG (cm^{-1})	WPRU1 (cm^{-1})
ν(O-H)	-	3523-3228	3296	3696-3113	3680-3113
ν(C=O)	-	-	1678	1720	1720
ν(C=N)	1680	1680	-	1643	1674
ν(C=C)	1613	1613	-	1606	1606
ν(Ar-Cl)	770	750	-	766	766
ν(Ar- F)	1139	1139	-	1145	1145

Powder X-ray diffraction patterns for WPRU1 MCC, WPRU1LAG, MDZ, MDZ·HCl and MP

PXRD patterns for the starting materials, WPRU1 and WPRU1 LAG samples were used to characterize the phases obtained from the ball milling experiment and final product of WPRU1. Furthermore, the WPRU1 calculated diffractogram was used to confirm that the WPRU1, and LAG phases were the same. The LAG diffractogram shares many similarities with both the WPRU1 and the WPRU1 calculated pattern. The profiles for the three samples correspond very well to peaks located at or near 2θ = 5.5, 7.3, 10.6, 18.4, 19.8, 23.3, 26.8, 29.3 and 30.6° (Figure 3.6). Minor differences in peak positions are due to the fact that the data for the experimental and calculated diffractograms were collected at different temperatures, 100K and 298K respectively. Differences in the intensities between the WPRU1, and WPRU1 LAG phases may be ascribed to some preferred orientation present in the WPRU1 diffractogram. The PXRD diffractograms of MP, MDZ and MDZ·HCl are significantly different from those of the WPRU1, LAG and the calculated diffractograms. The LAG pattern confirms a new phase formation obtained via mechanochemistry.

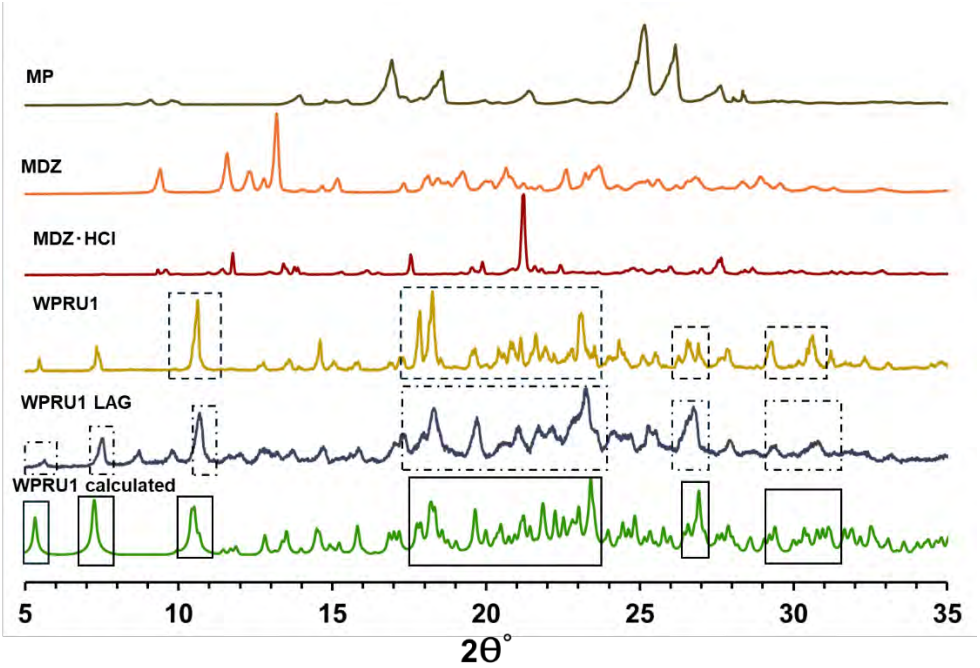

Figure 3.6 – Stacked PXRD patterns for WPRU1 cal., WPRU1 LAG, WPRU1, MDZ·HCl, MDZ and MP.

Thermal analysis of WPRU1 MCC, WPRU1 LAG, MDZ, MDZ·HCl and MP

Differential scanning calorimetry of MP (Figure 3.7) reveals that it melts in the range 125.4 – 128.2 °C, while MDZ melts in the range of 161.6 – 163.7 °C. The MDZ thermogram shows an additional broad endotherm in the range 55.0 – 125.0 °C due to dehydration since MDZ contains approximately 4.40% water, this was determined using TGA (see **Appendix Figure 1**). MDZ·HCl does not have a melting point as it undergoes decomposition when heated beyond 240.0 °C (see **Appendix Figure 2**). The WPRU1 MCC melts in the range 180.2 – 188.6 °C, and the WPRU1 LAG melts in the range 169.5 – 179.8 °C supporting evidence obtained from FTIR and PXRD. A summary of the onset and peak temperatures observed for the starting materials, WPRU1 MCC and WPRU1 LAG is listed in Table 3.5.

Table 3.5 – Melt onset and peak temperatures for WPRU1 MCC, MDZ, MDZ·HCl and MP.

Sample	T_{onset} (°C)	T_{peak} (°C)
MDZ	161.6	163.7
MDZ·HCl	240.0	
MP	125.4	128.2
WPRU1 MCC	180.2	188.6
WPRU1 LAG	169.5	179.8

The differences in the melting point ranges of WPRU1 LAG and WPRU1 MCC may be related to the presence of unreacted starting materials and the presence of small quantities of solvent in WPRU1 LAG.

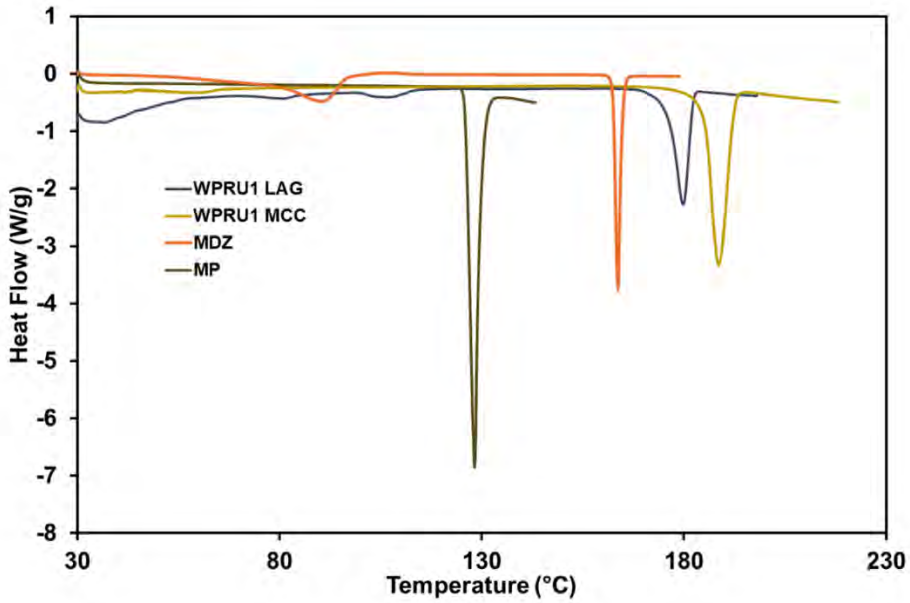

Figure 3.7 – DSC thermograms for MP, MDZ, MDZ·HCl, WPRU1 MCC, and LAG.

After identifying the single crystal as a salt formed between midazolam free base, midazolam HCl and methyl paraben, it inspired us to prepare other multicomponent crystals based on methyl paraben structural analogues with midazolam (free base).

3.3 MDZ·SA multicomponent crystal (Salt)

3.3.1 Introduction

The MDZ·SA LAG was prepared by grinding equimolar quantities of MDZ (0.49 mmol, 160 mg) and SA (0.49 mmol, 68 mg) using a mortar and pestle. 10 µl of methanol were added after grinding for 5 minutes, followed by an additional 10 minutes of grinding.

Single-crystal X-ray analysis of MDZ·SA MCC

Single crystals were prepared by dissolving the MDZ·SA LAG powder (8.0 mg) in 6 ml of diethyl ether. The solvent was added gradually whilst gently heating the solution to 25 °C to ensure that the solute was completely dissolved. The solution was filtered through a 0.45 µm nylon syringe filter into a vial and covered with a vial lid with a single hole to slow down evaporation. The solution was left to evaporate slowly under ambient conditions (22 °C, 101.3 kPa). A single crystal of good quality was selected for SCXRD characterization.

Data collection and space group determination

Unit cell parameters, crystal system, space group and single crystal data were collected on a Bruker D8 Venture diffractometer. A preliminary unit cell dimension check reveals that the MDZ·SA MCC crystallizes in the monoclinic space group $P2_1/c$.

Structure solution and refinement

Structure solution was performed using SHELXT[4] while structure refinement carried out using SHELXL[5]. Based on well-behaved isotropic temperature factors, all atoms were refined anisotropically, and hydrogen atoms were placed in idealized positions in a riding model. Peaks from a difference Fourier map were used to refine hydrogen atoms for heteroatoms. The data collection and refine parameters are summarized in Table 3.6.

Table 3.6 – Data-collection and refinement parameters for MDZ·SA MCC.

Data-collection and refinement parameters	
Formula unit	$(C_{18}H_{13}ClFN_3)(C_7H_6O_3)$
Formula mass (g mol^{-1})	463.88
Crystal system	Monoclinic
Space group	$P2_1/c$ (No. 14)
a/Å	12.4523(5)
b/Å	8.9474(3)
c/Å	19.5489(8)
α/°	90
β/°	94.828(2)
γ/°	90
Volume	2170.33(14)
Z	4
D_{calc} (g cm^{-3})	1.420
F (000)	960
μ (MoKα) (mm^{-1})	0.218
Crystal size (mm^3)	0.19 × 0.27 × 0.31
Temperature (K)	100(2)
Range scanned θ (°)	2.5 – 28.3
Index ranges	-16: 16; -11: 11; -26: 26
Total number of reflections collected	72728
Number of unique reflections	5387
Number of reflections with $I > 2\sigma(I)$	4436
Number of least-square parameters	308
R_{int}	0.072
S	1.03
R_1 (I>2σ (I))	0.0331
wR_2	0.0833
Weighting scheme parameters	a = 0.0329, b = 1.0650
$(\Delta/\sigma)_{mean}$	0.00
Δρ (e Å^{-3})	-0.26, 0.30

Molecular structure and noncovalent interactions

The asymmetric unit of MDZ·SA contains a single molecule of MDZ and a molecule of SA (Figure 3.8 (A)) with proton transfer between the carboxylic acid of SA and the imidazole ring of MDZ, Figure 3.8 (B). We were able to determine that proton transfer had occurred since we could model a hydrogen atom covalently bonded to the nitrogen atom N(32) of the imidazole ring. This conclusion is supported by the change in the specific bond lengths of the carboxylate group of SA and imidazole ring of MDZ. These values are tabulated in Table 3.7.

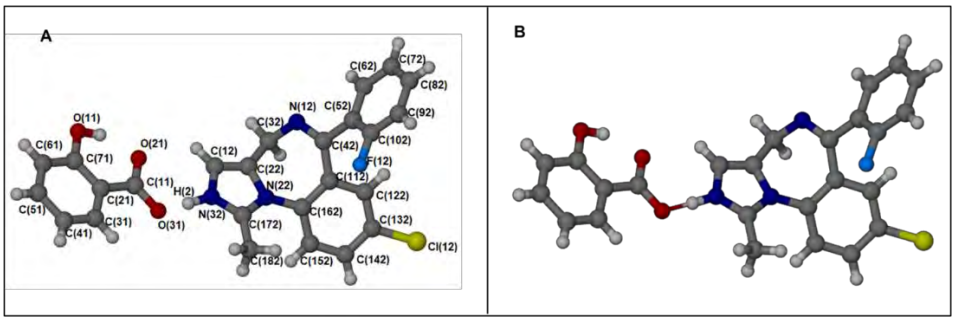

Figure 3.8 (A) – The labelled asymmetric unit of the MDZ·SA MCC. (B) shows the charge assisted hydrogen bonding between the carboxylate and imidazole moieties of MDZ·SA MCC.

Table 3.7 – Bond lengths of the carboxylate and imidazolium bonds in the MDZ·SA salt compared to the average bond lengths.

SA	Carboxylate bonds	Carboxylic acid bonds	Refcode
	This work		
C11-O21	1.2552(1)	1.257	SALIAC17[7]
C11-O31	1.2802(1)	1.277	
MDZ	**Imidazolium bonds**	**Imidazole bonds**	
C12-N32	1.3776(1)	1.383(3)	MOTGEI[8]
C172-N32	1.3231(1)	1.363(3)	

The MDZ and SA molecules interact with each other via a charge assisted N-H^{+}···O^{-} hydrogen bond between the protonated imidazole nitrogen atom N(32) of MDZ and the deprotonated oxygen atom O(31) of carboxylate moiety of SA, Figure 3.8 (B). The MDZ·SA MCC is therefore classified as a salt owing to proton transfer between these moieties. SA interacts with symmetry relate MDZ molecules via a carbonyl···π interaction between O(21) of the carboxylate moiety of SA and the imidazolium ring of MDZ (O(21)···C(12)-N(32)). The interaction distance is 3.53 Å. Two centro-symmetrically related MDZ molecules interact with each other via a halogen···π interaction F(12)···[$C(52)–$C(102)$F(12)] between the fluorophenyl rings having an interaction distance of 3.31 Å as depicted in Figure 3.9. The hydrogen bond parameters for the MDZ·SA salt are summarised in Table 3.8.

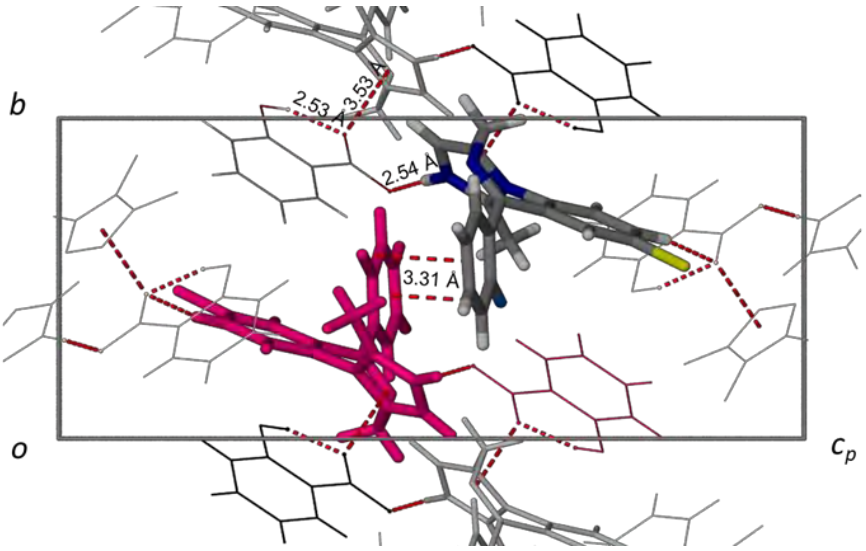

Figure 3.9 – A view down the a axis showing only the most pertinent noncovalent interactions.

Table 3.8 – Hydrogen bond parameters for MDZ·SA MCC.

D-H···A	D···A (Å)	D-H···A (°)	Symmetry Code
O11-H1···O21	2.5343(1)	154.00	intramolecular bond
N32-H2···O31	2.5429(1)	174.00	1-x,1-y, -z
C41-H41···F12	3.2617(1)	133.00	x, 1+y, z
C82-H82···N32	3.4828(1)	151.00	-x, -y, -z
C142-H142···O21	3.2586(1)	155.00	1-x, -1/2+y, 1/2-z
C152-H152···O11	3.2671(1)	133.00	-
F(12)···[$C(52)–$C(102)$F(12)]	3.3145(1)	97.81	2-x,1-y,1-z
O(21)···[C(11)-N(32)]	3.5306(1)	74.82	1-x,2-y,1-z

The mean F···π and O···π interaction distances as determined from a CSD survey are 3.576 ± 0.149 Å and 3.858 ± 0.203 Å, respectively.[9]

Crystal Packing

In the structure, MDZ·SA units are noncovalently bonded via a halogen···π interaction to a centro-symmetrically related MDZ·SA unit. In turn, the halogen···π bonded dimers stack diagonally along the [5 0 3] direction and are hydrogen bonded (C(142)-H(142)···O(21)) to successive halogen bonded dimers. Successive diagonal layers are hydrogen bonded to each other through the charge assisted hydrogen bond interaction between the MDZ and SA molecules as depicted in Figure 3.10.

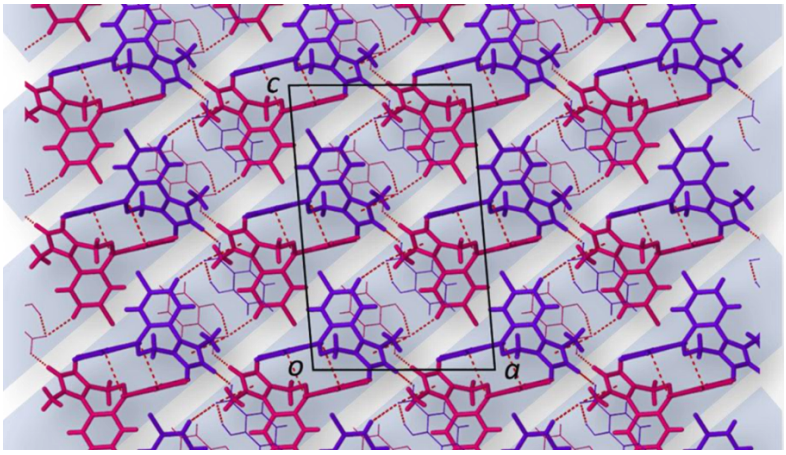

Figure 3.10 – View along the b axis of showing the diagonal layers. The centro symmetric molecules are coloured purple and pink for clarity while successive diagonal layers are highlighted in blue.

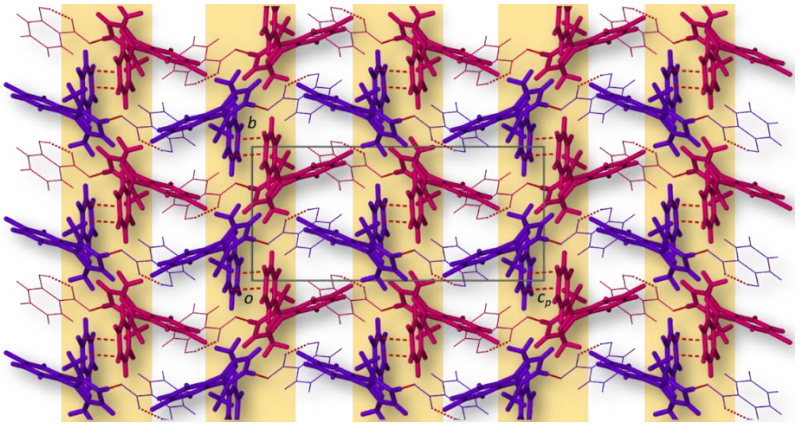

Figure 3.11 – View down the a axis showing the columns of centrosymmetric MDZ·SA dimers that are stacked parallel to the b axis.

When viewed down the *a* axis, Figure 3.11, the centrosymmetric MDZ·SA dimers are stacked in columns parallel to the *b* axis. Consecutive columns are hydrogen bonded to each other through a (C(142)-H(142)···O(21)) interaction and are interspersed by SA molecules.

3.3.2 Bulk characterization

FTIR spectra for MDZ·SA MCC, MDZ·SA LAG, MDZ and SA samples

The FTIR spectra for the starting, LAG and recrystallised materials were measured and used as a basis for identifying formation of a new phase. These spectra are illustrated in Figure 3.12.

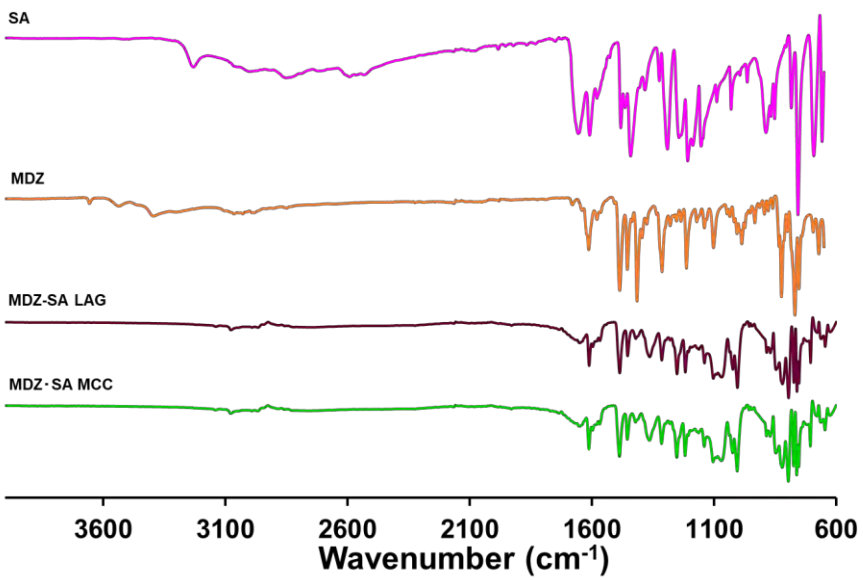

Figure 3.12 – FTIR spectra for salicylic acid (SA), midazolam (MDZ), MDZ·SA LAG, and the recrystallised sample.

The FTIR spectrum of the pure SA showed characteristic vibrational modes at 3231 cm^{-1} and between 3006-2852 cm^{-1}, which are assigned to ν(O-H) stretching bands, respectively. The peaks observed at 1656 cm^{-1} and 1382 cm^{-1} are both assigned to the ν(C=O) vibrational mode, while the peak at 1612 cm^{-1} is attributed to ν(C=C) stretching. Furthermore, the COO^-(C-O) stretching and C-OH stretching were assigned to peaks that appeared at 1292 cm^{-1} and 1208 cm^{-1} respectively, which are in agreement with the literature.[10] The MDZ spectrum is characterized by a low intensity imine band ν(C=N) occuring at 1680 cm^{-1}, an aromatic ν(C=C) strectch at 1613 cm^{-1} and two aryl halide bands ν(Ar-F) at 1139 cm^{-1} and ν(Ar-Cl) at 770 cm^{-1}. In the spectrum of the LAG and recrystallised products, the carbonyl peaks are shifted. The ν(C=O) band at 1382 cm^{-1} shifts due to proton transfer from the carboxylic acid moiety of SA to the imidazole moiety on MDZ. The charge assisted hydrogen bond formation between these groups, $N\text{-}H^+\cdots O^-$, contributes to the shift. Vibrational modes of pertinent groups are reported in Table 3.9.

Table 3.9 – Vibrational modes for the MDZ·SA MCC, MDZ·SA LAG, MDZ and SA samples.

Vibrational Modes	MDZ (cm^{-1})	SA (cm^{-1})	MDZ·SA LAG (cm^{-1})	MDZ·SA MCC (cm^{-1})
ν(O-H)	-	3006-2852	-	-
Carboxylic ν(O-H)	-	1208	1217	1217
ν(O-H)	-	3231	2419	2419
ν(C=O)	-	1656 and 1382	1648 and 136	1648 and 1363
ν(C=N)	1680	-	-	-
ν(Ar-Cl)	770	-	-	-
ν(Ar-F)	1139	-	-	-

PXRD patterns for MDZ·SA MCC, MDZ·SA LAG, MDZ and SA

PXRD patterns of MDZ and SA were used to compare against the PXRD profiles of MDZ·SA MCC, MDZ·SA LAG and the MDZ·SA calculated pattern (Figure 3.13). It is clear from the diffractograms that the starting materials do not match the LAG or recrystallised material. Moreover, the LAG, MCC and calculated profiles are very similar and have a high level of correspondence.

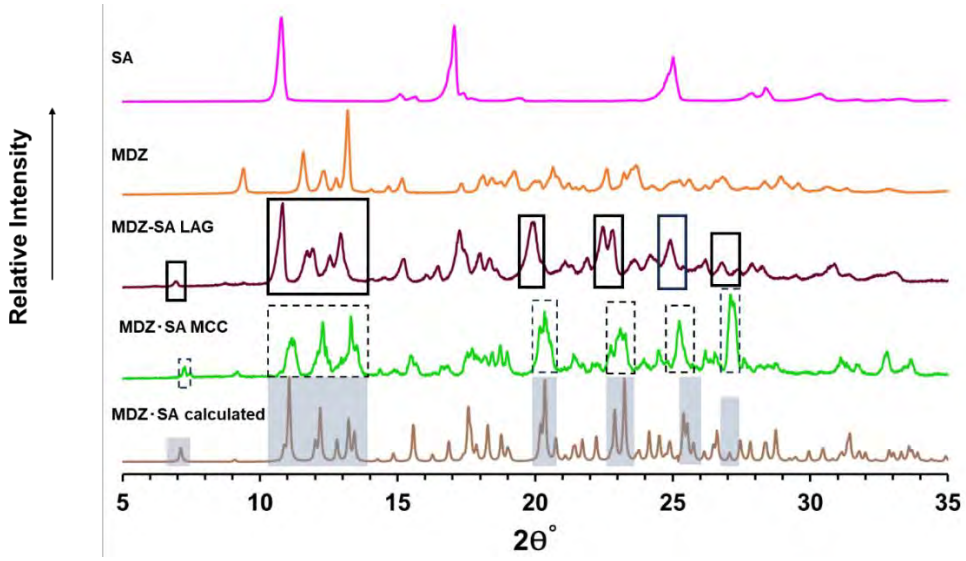

Figure 3.13 – Powder patterns of the starting materials, LAG, MDZ·SA MCC and calculated pattern for MDZ·SA MCC.

The three diffractograms are very well matched in the areas highlighted by the shaded or enclosed region. The minor differences in peak position between the LAG and MCC diffractograms may be due to differences in the temperature at which the data were collected. The differences in peak intensity may be due to prefered orientation.

Thermal analysis of MDZ·SA MCC, MDZ·SA LAG, MDZ and SA

The melting ranges for SA and MDZ obtained from differential scanning calorimetry are 158.1 – 161.1 °C and 161.6 – 163.7 °C, respectively (Figure 3.14). The DSC thermograms for the LAG and recrystallised samples of MDZ·SA are virtually identical and both display a single melting endotherm in the range 157.1 – 163.1 °C. These values are also very similar to values for MDZ, except that MDZ has a second endotherm resulting from water loss.

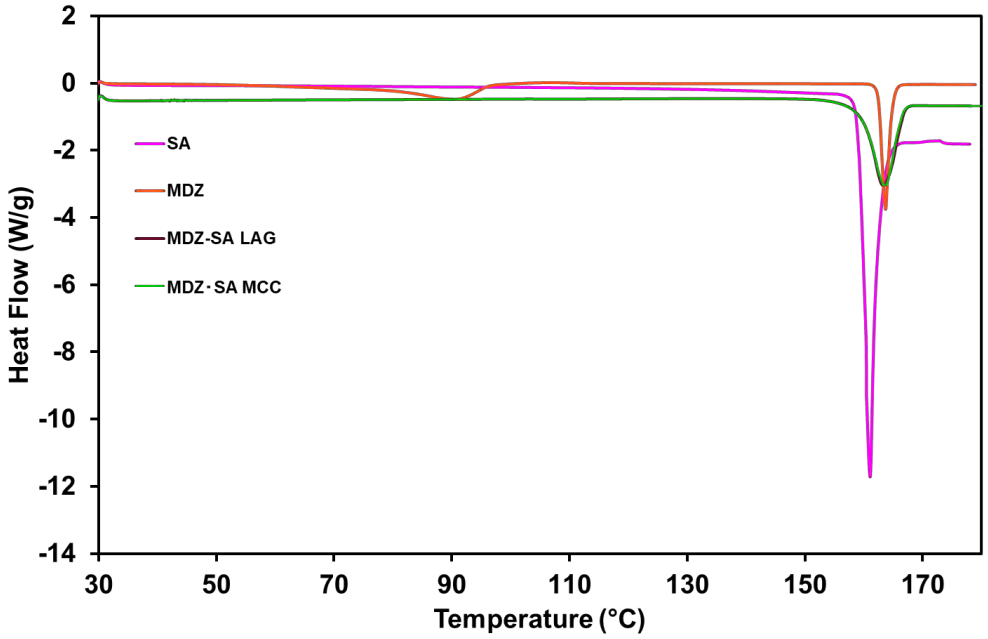

Figure 3.14 – DSC curves of SA, MDZ, MDZ·SA LAG and MDZ·SA MCC.

The onset and peak temperatures of the starting materials, LAG, and MCC are reported in Table 3.10.

Table 3.10 – Melt onset and peak temperatures for the starting materials, LAG, and MDZ·SA MCC.

Sample	T_{onset} (°C)	T_{peak} (°C)
MDZ	161.6	163.7
SA	158.1	161.1
MDZ·SA LAG	157.1	163.1
MDZ·SA MCC	157.1	163.1

3.4 Summary

Based on our numerous attempts to recreate the WPRU1 MCC, we successfully isolated and fully characterized two multicomponent salts viz., WPRU1 and MDZ-SA. The WPRU1 MCC could only be prepared using mechanochemistry, while MDZ-SA could be prepared both mechanochemistry and slow evaporation. An extensive search in the CSD[9] revealed that neither of these salts have previously been reported.

3.5 References

1 Bhatt-Mehta V., Rosen D.A., King S., and Maksym C.J., Stability of parenteral midazolam in an oral formulation. *Am J Hosp Pharm*., **1993**, 50, 285–288.

2 Mandrioli R., Mercolini L., and Raggi M.A., Benzodiazepine Metabolism: An Analytical Perspective. *Curr Drug Metab*., **2008**, 9, 827–844.

3 Olkkola K.T., and Ahonen J., Midazolam and Other Benzodiazepines. *Handb Exp Pharmacol*., **2008**, 182. 335-360.

4 Sheldrick G.M. SHELXT - Integrated Space-Group and Crystal-Structure Determination. *Acta Crystallogr A.,* **2015**, *71* (1), 3–8.

5 Sheldrick G. M. Crystal Structure Refinement with SHELXL. *Acta Crystallogr C Struct Chem.,* **2015**, *71*, 3–8.

6 Sateesh Babu J.M., Sevukarajan M., Thamizhvanan K., Naveenkumar B., Bandaru S., Reddy B.S., Vivekananda U., and Shyamkumar V., Evaluation of Physicochemical and Anti-tubercular Activity of Co-crystal of Isoniazid with Methyl Paraben. *IJIDD.,* **2013**, 3, 10-27.

7 Montis R., and Hursthouse M.B., Surprisingly complex supramolecular behaviour in the crystal structures of a family of mono-substituted salicylic acids. *CrystEngComm*., **2012**, 14, 5242–5254.

8 Chen Y., Guo J., Huang X., Yun R., and Wu H., 2,6-Bis(1H-benzimidazol-2-yl)pyridine methanol trisolvate. *Acta Crystallogr Sect E Struct Rep Online*., **2009**, 65, 1013.

9 Ferrence G.M., Tovec C.A., Holgate S.J.W., Johnson N.T., Lightfoot M.P., Nowakowska-Orzechowska K.L., Ward S.C., CSD Communications of the Cambridge Structural Database, *IUCrJ.*, **2023**, 10, 6-15.

10 Guan X-H., Guang-Hao C. and Chii S., ATR-FTIR and XPS study on the structure of complexes formed upon the adsorption of simple organic acids on aluminium hydroxide, *J. Environ. Sci.,* **2007**,19, 438-443.

Chapter 4: Midazolam Multicomponent Crystals (Co-crystals)

In this chapter we report co-crystals prepared using midazolam free base and structural analogues of MP *viz*., benzoic acid (BA), 3-hydroxybenzoic acid (3-HBA) and *p*-aminobenzoic acid (PABA).

4.1 MDZ·BA multicomponent crystal

4.1.1 Introduction

The MDZ·BA LAG experiment was prepared by grinding equimolar quantities of MDZ (0.49 mmol, 160 mg) and BA (0.49 mmol, 60 mg) together, using a mortar and pestle. 10 µl of methanol was added after grinding for 5 minutes, followed by an additional 10 minutes of grinding.

Single-crystal X-ray analysis of MDZ·BA MCC

Single crystals were prepared by dissolving the MDZ·BA LAG powder (8.2 mg) in approximately 7 ml diethyl ether. The solvent was added gradually whilst gently heating the solution to 25 °C to ensure full dissolution. The solution was filtered through a 0.45 µm nylon syringe filter into a vial and covered with a vial lid with a single hole to ensure slow evaporation. The sample was left to evaporate under ambient conditions (22 °C, 101.3 kPa). A single crystal of suitable quality was chosen for SCXRD analysis.

Data collection and space group determination

Unit cell parameters, crystal system, space group and single crystal data were collected on a Bruker D8 Venture diffractometer. A preliminary unit cell dimension check reveals that the MDZ·BA MCC crystallizes in the triclinic system, in the space group *P* -1.

Structure solution and refinement

The structure for MDZ·BA MCC was solved using SHELXT[1] and refined using SHELXL[2]. Based on well-behaved isotropic temperature factors, all atoms were refined anisotropically, and hydrogen atoms were placed in idealized positions in a riding model. Peaks from the difference Fourier map were used to refine hydrogen atoms associated to heteroatoms. Data collection and refine parameters are summarized in Table 4.1.

Table 4.1 – Data-collection and refinement parameters for MDZ·BA MCC.

Data-collection and refinement parameters	
Formula unit	$(C_{18}H_{13}ClFN_3)(C_7H_6O_2)$
Formula mass (g mol^{-1})	447.88
Crystal system	Triclinic
Space group	*P* -1 (No. 2)
a/Å	8.1804(10)
b/Å	11.1597(13)
c/Å	12.2430(16)
α/°	90.198(5)
β/°	91.052(5)
γ/°	105.042(4)
Volume	1079.2(2)
Z	2
D_{calc} (g cm^{-3})	1.378
F (000)	464
μ (MoKα) (mm^{-1})	0.214
Crystal size (mm^3)	0.31 × 0.52 × 0.66
Temperature (K)	100(2)
Range scanned θ (°)	2.5 – 27.1
Index ranges	-10: 10; -14: 14; -15: 15
Total number of reflections collected	15841
Number of unique reflections	4711
Number of reflections with $I > 2\sigma(I)$	3329
Number of least-square parameters	295
R_{int}	0.088
S	1.07
R_1 (I>2σ (I))	0.0816
wR_2	0.2337
Weighting scheme parameters	a = 0.1141, b = 2.2440
$(\Delta/\sigma)_{mean}$	0.00
Δρ excursions (e Å^{-3})	-0.77, 0.55

Molecular structure and noncovalent interactions

The asymmetric unit depicted in Figure 4.1 (A) contains a single molecule of MDZ and a single molecule BA that are hydrogen bonded to each other via an O-H···N hydrogen bond between the hydroxyl moiety of the carboxylic acid O(11)-H(9) and the imidazole nitrogen atom N(22), as shown in Figure 4.1 (B).

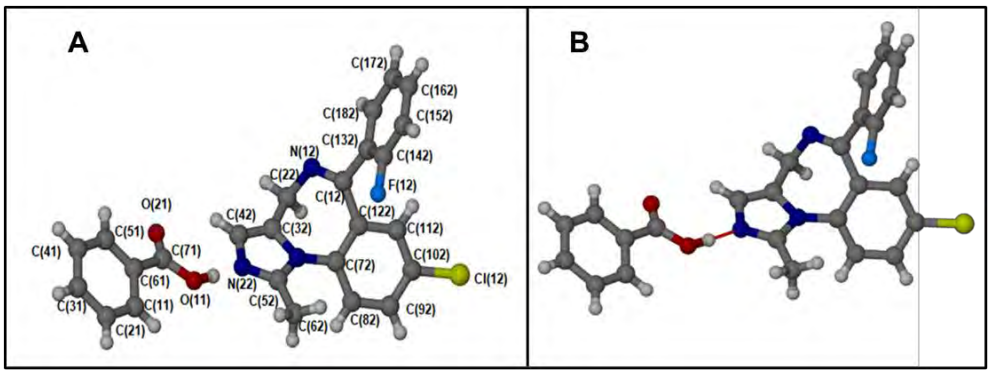

Figure 4.1 – (A) The labelled asymmetric unit of MDZ·BA MCC and (B) showing the hydrogen bonding interaction between MDZ and BA.

Some of the noncovalent interactions that span the crystal, parallel to the *b* axis are depicted in Figure 4.2. These interactions include the aforementioned O-H···N hydrogen bond between BA and MDZ, a halogen···π interaction F(12)···[$C(132)–$C(182)$F(12)] between symmetry related MDZ free base molecules and a weak C(92)-H(92)···O(21) hydrogen bond between a hydrogen atom on the chlorophenyl ring of MDZ and the carbonyl oxygen atom of the carboxylic acid moiety of BA.

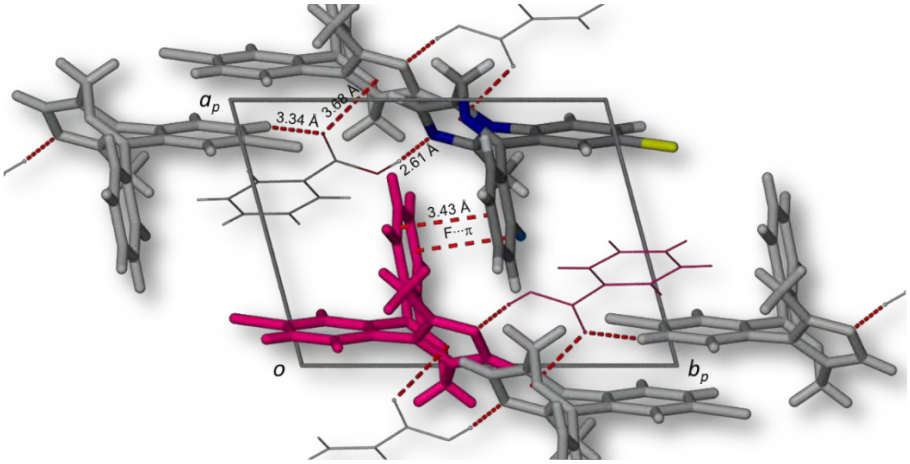

***Figure 4.2 – Hydrogen bonding and* fluorine···π and Carbonyl···π interactions viewed down the *c* axis. Only the most *relevant* interactions are shown for clarity.**

The halogen···π interaction distance is 3.43 Å while the carbonyl···π interaction distance is 3.68 Å. More precise noncovalent data are presented in Table 4.2.

Table 4.2 – *Noncovalent interaction parameters for MDZ·BA MCC*.

D-H···A	D···A (Å)	D-H···A (°)	Symmetry Code
O11-H9···N22	2.611(4)	174.0(5)	-
C92-H92···O21	3.338(4)	165.0	X,1+Y, Z
C162-H162···N22	3.512(5)	166.0	1-X,1-Y,-Z
F(12)···[$C(132)–$C(182)$F(12)]‡	3.430(2)	86.18(17)	1-X,1-Y,-Z
O(21)···[C(32)-C(42)-C(52)-N(22)-N(32)]§	3.684(3)	68.78(19)	2-X,1-Y,1-Z

The mean F···π and O···π interaction distances as determined from a CSD survey are 3.576 ± 0.149 Å and 3.858 ± 0.203 Å, respectively.[3]

Crystal Packing

The packing arrangement of MDZ·BA MCC is characterised by columns of MDZ molecules that are parallel to the *a* axis and stacked along the *b* axis, see Figure 4.3. Each column consists of pairs of MDZ molecules that are centro-symmetrically related and held together by noncovalent halogen···π interactions. The centro-symmetrically pairs are, in turn, translated along the ([100]) direction. The columns of MDZ molecules are separated by BA molecules which are hydrogen bonded to the MDZ molecules.

‡ [$C(132)–$C(182)] is shorthand for the symmetry related ring involving atoms C132-C142-C152-C162-C172-C182.

§§§[C(32)-C(42)-C(52)-N(22)-N(32)] is a five membered ring.

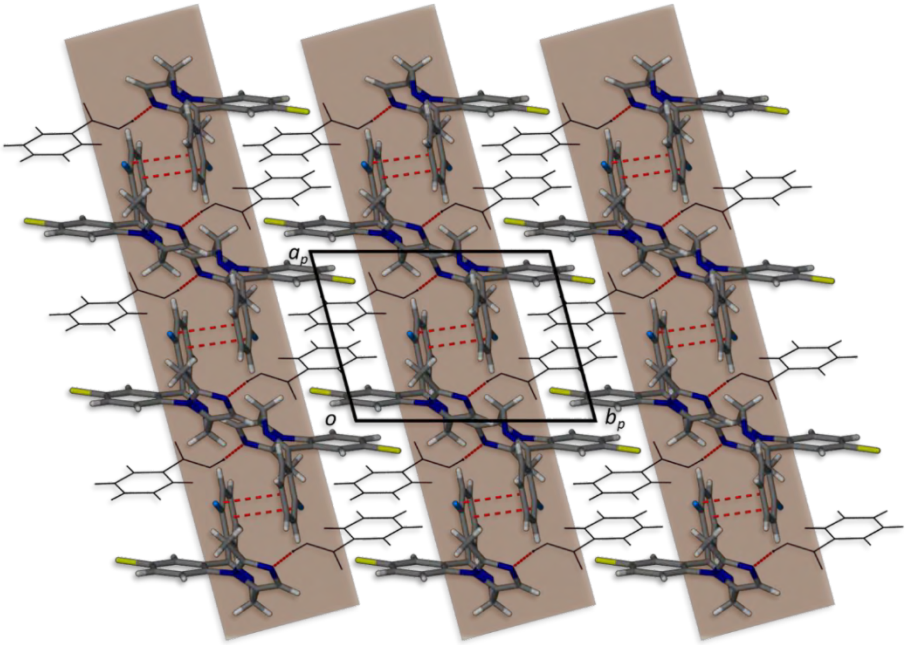

Figure 4.3 – Columns of MDZ·BA molecules stacked along the b axis. A single layer of molecules is shown for the purposes of clarity.

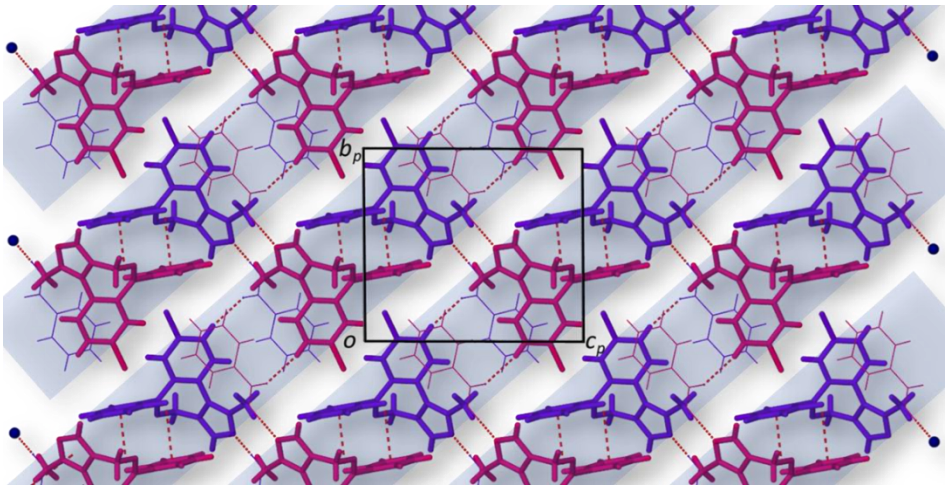

Figure 4.4 – A single layer of MDZ·BA MCC view onto the bc plane.

When viewed down the *a* axis, it is evident that the MDZ·BA molecules are hydrogen bonded in sheets that are parallel to the [0 1 1] direction as depicted in Figure 4.4. Successive layers are linked via the O(11)-H(9)···N22 hydrogen bond formed between an MDZ molecule in one layer and a BA molecule in another.

4.1.2 Bulk characterization

FTIR spectra for MDZ·BA MCC, MDZ·BA LAG, MDZ and BA samples

The individual starting materials were analyzed using FTIR spectroscopy, and the spectra were used as a reference to establish MCC formation. These spectra are presented in Figure 4.5, alongside the spectra for the LAG sample and the bulk crystalline material.

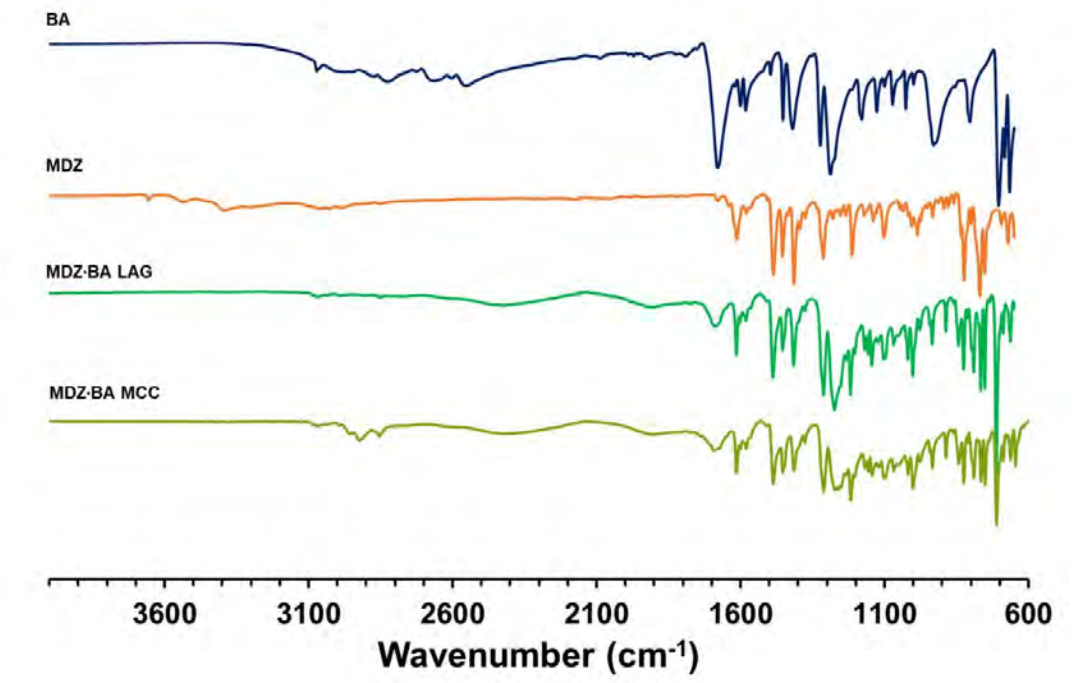

Figure 4.5 – FTIR spectra of benzoic acid (BA), midazolam (MDZ), MDZ·BA LAG, and the recrystallised sample.

The BA spectrum exhibts a broad ν(O-H) band between 3071-2500 cm^{-1}. The bands at 1679 and 1323 cm^{-1} are attributed to ν(C=O) and ν(O-H) of the carboxylic acid consistent with values reported in literature.[4] The MDZ spectrum is characterized by a low intensity imine band ν(C=N) occuring at 1680 cm^{-1}, an aromatic ν(C=C) strectch at 1613 cm^{-1} and two aryl halide bands ν(Ar-F) at 1139 cm^{-1} and ν(Ar-Cl) at 770 cm^{-1}. The MDZ·BA MCC and LAG spectra are very similar, hence only the MDZ·BA MCC spectrum was analyzed however, the vibrational modes for the LAG sample are reported in Table 4.3. The spectrum for MDZ·BA MCC shows that the carbonyl stretching bands are shifted from where they occur in pure BA (see Table 4.3). The carbonyl stretch ν(C=O) at 1679 cm^{-1} shifts to 1693 cm^{-1} due to a O-H···N hydrogen bonding interaction. A new broad absorption peak centered at the wavenumber 2419 cm^{-1} indicates the presence of hydrogen bonding in the structure. A summary of the vibrational modes is reported in Table 4.3.

Table 4.3 – ***Vibrational modes for the MDZ·BA MCC, MDZ·BA LAG, BA and MDZ samples.***

Vibrational Modes	MDZ (cm^{-1})	BA (cm^{-1})	MDZ·BA LAG (cm^{-1})	MDZ·BA MCC (cm^{-1})
ν(O-H)	-	3071-2500	-	-
Carboxylic ν(O-H)	-	1323	1311	1312
ν(O-H)	-	-	2422	2419
ν(C=O)	-	1679	1688	1693
ν(C=N)	1680	-	-	-
ν(C=C)	1613	-	-	-
ν(Ar-Cl)	770	-	-	-
ν(Ar- F)	1139	-	-	-

PXRD patterns for MDZ·BA MCC, MDZ·BA LAG, MDZ and BA

PXRD patterns for the starting materials, MDZ·BA MCC and MDZ·BA LAG samples were used to characterize the phases obtained from the grinding and recrystallisation experiments. Furthermore, the MDZ·BA calculated diffractogram was used to confirm that the MDZ·BA MCC, and MDZ·BA LAG phases were the same. The LAG diffractogram shares many similarities with both the MDZ·BA MCC and the MDZ·BA calculated pattern. The profiles for the three samples correspond very well to peaks located at or near 2θ = 7.1, 10.7, 14.0, 21.5 and 23.9° (Figure 4.6). The slight differences in peak positions are due to the fact that the data for the experimental and calculated diffractograms were collected at different temperatures. Differences in the intensities between MDZ·BA MCC, and MDZ·BA LAG phases may be ascribed to some preferred orientation present in the MDZ·BA MCC diffractogram. This is evidenced by the low intensity of the peaks located at 2θ = 7.1, and 10.7° in the MDZ·BA MCC diffractogram (enclosed by the dashed line boxes, Figure 4.6). The characteristic diffraction peaks for BA and MDZ are as previously reported. Both the LAG and MCC patterns confirm new phase formation.

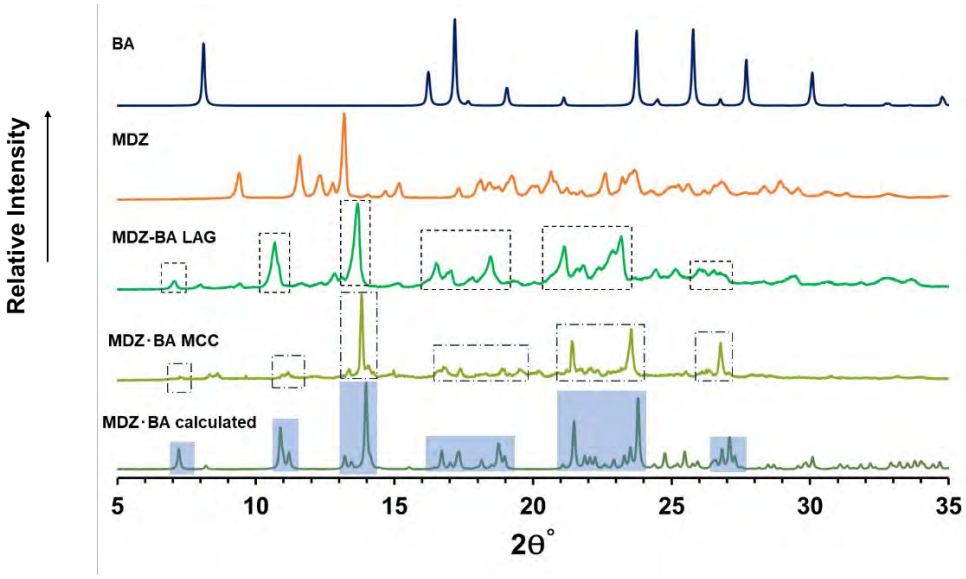

Figure 4.6 – Stacked PXRD patterns for MDZ·BA cal., MDZ·BA MCC, MDZ·BA LAG, MDZ and BA.

Thermal analysis for MDZ·BA MCC, MDZ·BA LAG, MDZ and BA samples

BA melts in the range 123.2 – 124.8 °C while MDZ melts in the range 161.6 – 163.7 °C, consistent with previous reports. The LAG sample melts in the range 124.4 – 129.4 °C, different from the starting materials BA and MDZ. The MDZ·BA MCC has a single broad endotherm with an onset temperature of 125.3 °C different from the starting materials but similar to the LAG melting range. The slight difference in the peak positions is possibly due to particle size of the respective samples. Both the LAG and MDZ samples have broad endotherms in the range 55.0 to 108.2 °C, which correlates to solvent loss. In the case of the

LAG sample, the solvent is methanol whereas for the MDZ sample it is water. The TGA thermograms of the LAG and MDZ samples reflect a weight loss of 1.64% and 4.40% respectively. These TGA thermograms have been included in **Appendix Figures 1 and 3**. The melt endotherms for the LAG and MCC samples differ from those of the starting materials, which is indicative of a new phase formation as depicted in Figure 4.7.[5] The onset and peak temperatures for the starting materials, LAG, and MCC samples are summarised in Table 4.4.

Table 4.4 – Melt onset and peak temperatures for MDZ·BA MCC, MDZ·BA LAG, MDZ and BA samples.

Sample	T_{onset} (°C)	T_{peak} (°C)
BA	123.2	124.8
MDZ	161.6	163.7
MDZ·BA LAG	124.4	129.4
MDZ·BA MCC	125.3	131.8

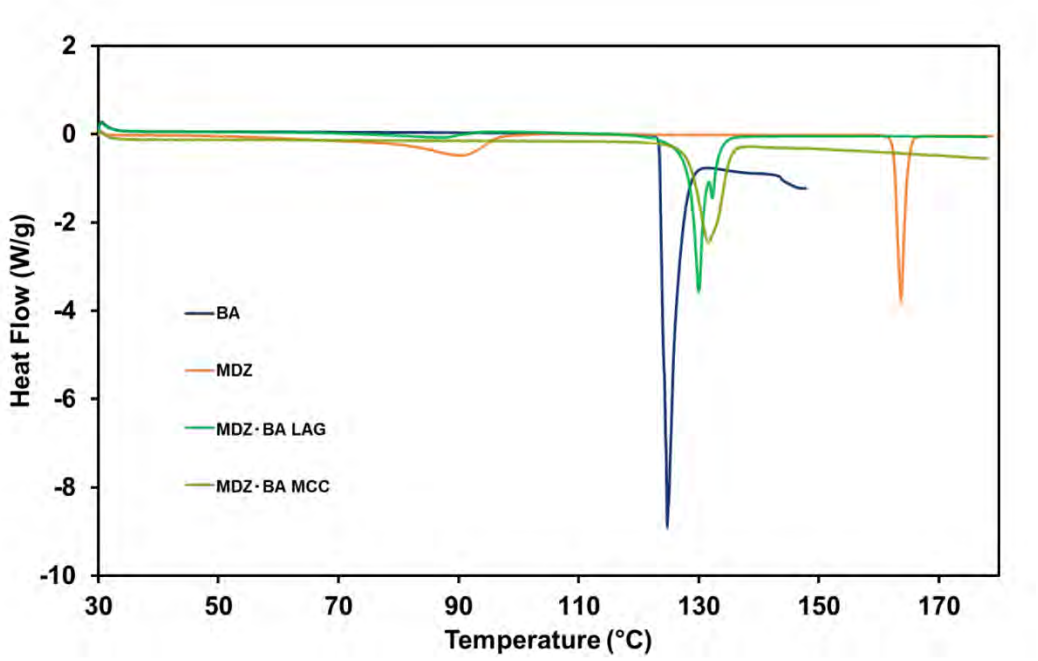

Figure 4.7 – DSC thermograms for BA, MDZ, MDZ·BA LAG and MDZ·BA MCC samples.

4.2 MDZ·3-HBA MCC

4.2.1 Introduction

The MDZ·3-HBA LAG was prepared by grinding equimolar quantities of MDZ (0.49 mmol, 160 mg) and 3-HBA (0.49 mmol, 68 mg) using a mortar and pestle. 10 µl of methanol were added after grinding for 5 minutes, followed by an additional 10 minutes of grinding.

Single-crystal X-ray analysis of MDZ·3-HBA MCC

Single crystals of MDZ·3-HBA were prepared by dissolving 8.4 mg of MDZ·3-HBA LAG in 8 ml of diethyl ether. The solvent was added gradually whilst gently heating the solution to 25 °C to ensure that the solute was fully dissolved. The solution was filtered through a 0.45 µm nylon syringe filter into a vial and covered with a vial lid with a single hole to slow down evaporation. The sample was left to evaporate slowly under ambient conditions. A suitable single-crystal was chosen for SCXRD characterization.

Data collection and space group determination

A Bruker D8 Venture diffractometer was used to collect single-crystal data for each crystal. The unit cell parameters, crystal system, and space group were determined using single-crystal X-ray diffraction. A preliminary unit cell dimension check reveals that the MDZ·3-HBA MCC crystallizes in the triclinic crystal system in the space group *P*-1.

Structure solution and refinement

Structure solution was carried out using SHELXT[1] and SHELXL[2] was used for structure refinement. Based on well-behaved isotropic temperature factors, all atoms were refined anisotropically, and hydrogen atoms were placed in idealized positions in a riding model. Peaks from the difference Fourier map were used to refine hydrogen atoms for heteroatoms. Data collection and refine parameters are reported in Table 4.5.

Table 4.2 – Data-collection and refinement parameters for MDZ·3-HBA MCC.

Data-collection and refinement parameters	
Formula unit	$(C_{18}H_{13}ClFN_3)(C_7H_6O_3)$
Formula mass (g mol^{-1})	463.88
Crystal system	Triclinic
Space group	*P* -1 (No. 2)
a/Å	7.6237(3)
b/Å	12.0258(5)
c/Å	12.2463(5)
α/°	90.2620(10)
β/°	99.0040(10)
γ/°	102.3690(10)
Volume	1082.33(8)
Z	2
D_{calc} (g cm^{-3})	1.423
F (000)	480
μ (MoKα) (mm^{-1})	0.219
Crystal size (mm^3)	0.22 × 0.29 × 0.40
Temperature (K)	100(2)
Range scanned θ (°)	2.4 – 27.1
Index ranges	-9: 8; -15: 15; -15: 15
Total number of reflections collected	48113
Number of unique reflections	4762
Number of reflections with $I > 2\sigma(I)$	4181
Number of least-square parameters	303
R_{int}	0.043
S	1.06
R_1 (I>2σ (I))	0.0433
wR_2	0.1144
Weighting scheme parameters	a = 0.0507, b = 1.05290
$(\Delta/\sigma)_{mean}$	0.00
Δρ excursions (e Å^{-3})	-0.39, 0.96

Molecular structure and noncovalent interactions

The asymmetric unit shown in Figure 4.8 (A) contains a molecule of MDZ and a molecule of 3-HBA that are hydrogen-bonded via the hydroxyl moiety of the carboxylic acid of 3-HBA to the imidazole ring of MDZ, as shown in Figure 4.8 (B).

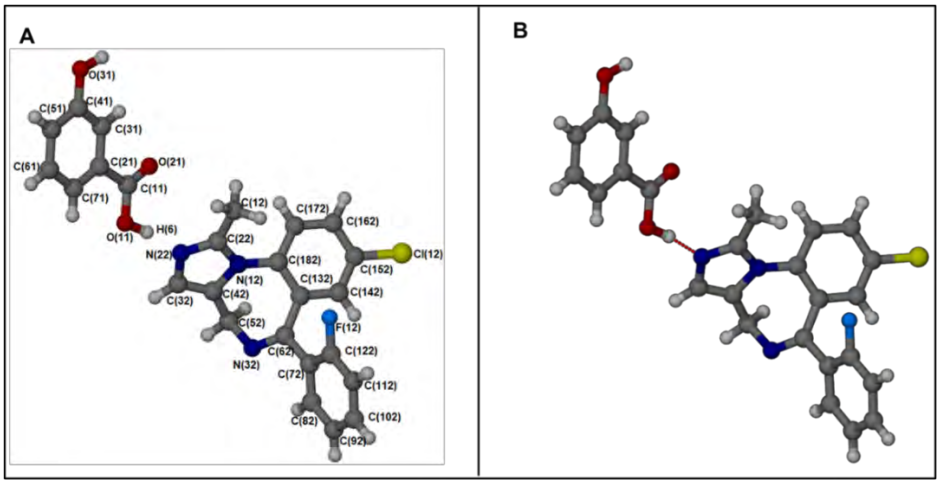

Figure 4.8 (A) – Labelled asymmetric unit of the MDZ·3-HBA MCC and (B) – the hydrogen bonded asymmetric unit of the MDZ·3-HBA MCC.

3-HBA hydrogen bonds to two different MDZ molecules via two O-H···N intermolecular hydrogen bonds. MDZ also interacts with 3-HBA via a C-H···π interaction formed between a hydrogen atom on the fluorophenyl ring of MDZ (C(112)-H(112)) and the phenyl ring of 3-HBA [C(21)-C(31)-C(41)-C(51)-C(61)-C(71)]. Furthermore, each MDZ molecule is halogen bonded (Cl12···F12) to a symmetry translated MDZ molecule with an interaction distance of 3.05 Å. Some of the noncovalent interactions are highlighted in Figure 4.9 and the noncovalent interaction parameters are reported in Table 4.6.

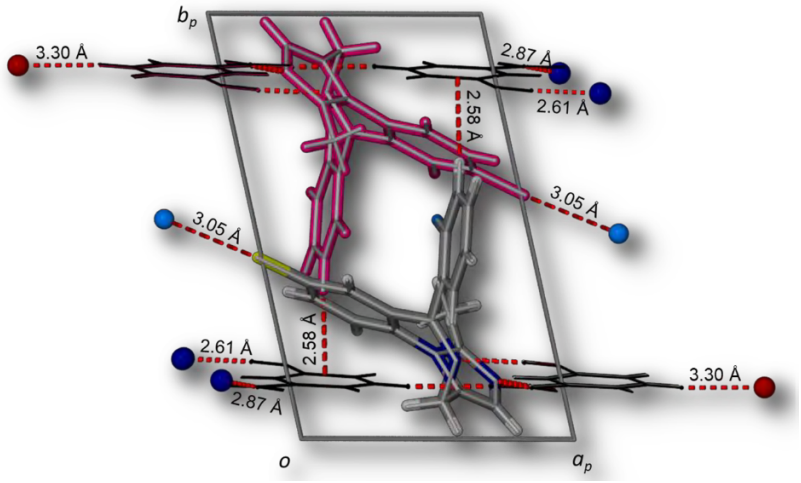

Figure 4.9 – View down the c axis showing some of the noncovalent interaction present in the structure.

Table 4.6 – Noncovalent interaction parameters for MDZ·3-HBA MCC.

D-H···A	D···A (Å)	D-H···A (°)	Symmetry Code
O31-H3···N32	2.871(2)	172(3)	x, y, 1+z
O11-H6···N22	2.608(2)	172(3)	-
C61-H61···O21	3.301(2)	168.0	-1+x, y, z
Cl12···F12	3.0495(12)	175.02(6)	1+x, y, z
C(112)-H(112)···[C(21)-C(71)]**	2.580	146.00	-x, 1-y, 1-z
[C(21)-C(71)]···[$C(21)-$C(71)]††	3.5713(10)	-	-x, 2-y, 2-z

Crystal Packing

The packing arrangement of MDZ·3-HBA MCC viewed down the *a* axis is depicted in Figure 4.10. The MDZ·3-HBA units are arranged in centro-symmetric pairs, indicated by the pink and purple molecules (Figure 4.10), which are stacked in layers parallel to the *c* axis. The 3-HBA molecules are hydrogen bonded to two consecutive MDZ molecules forming a bilayer either side of the layer of centro-symmetric MDZ pairs. The bilayers of 3-HBA molecules are in π···π contact within the layer while there are C-H···π interactions linking the 3-HBA molecules to the MDZ molecules, see Figure 4.10 and Table 4.6. Consecutive layers are stacked along the *b* direction.

** [C(21)-C(71)] is shorthand for the ring involving atoms C21-C31-C41-C51-C61-C71.
†† [$C(21)-$C(71)] is shorthand for the symmetry related ring involving atoms C21-C31-C41-C51-C61-C71.

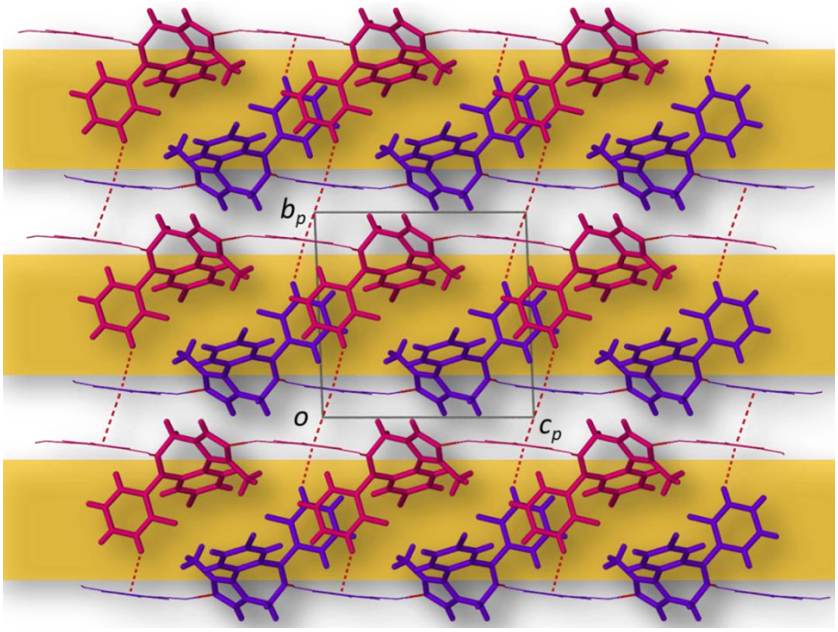

Figure 4.10 – View down the a axis showing the parallel layers of MDZ·3-HBA pairs. Also Shown here are the C-H···π interactions between MDZ and 3-HBA and the π···π interactions between two 3-HBA molecules.

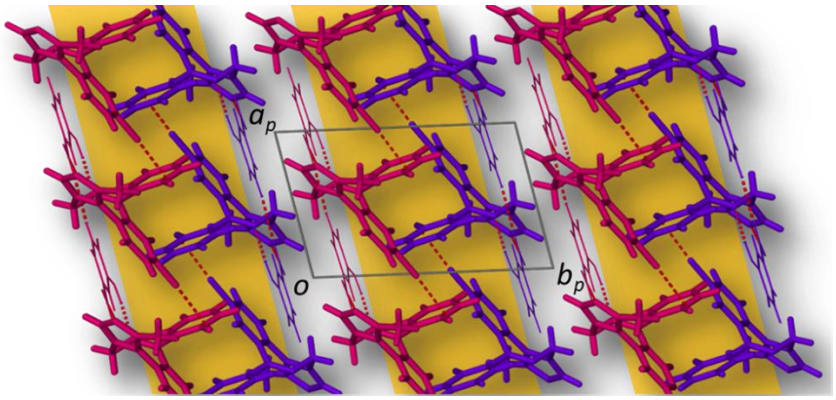

Figure 4.11 – View down the c axis of MDZ·3-HBA showing the parallel columns of centrosymmetric pairs.

When viewed down the *c* axis, the centrosymmetric pairs stack in columns parrallel to the *a* axis. Consective pairs interact via a halogen bond formed between the chlorine atom of an MDZ molecule and the fluorine atom of a centrosymmetrically related MDZ molecule (Cl12···F12), see Figure 4.11. These halogen bond interactions are intra-column and are parallel to [1 0 0].

4.2.2 Bulk characterization

FTIR spectra of MDZ·3-HBA LAG sample, starting and crystalline materials

The individual starting materials along with the milled and recrystallised materials were characterised using FTIR spectroscopy. The spectra of the starting materials were used as a reference for identifying new phase formation and all spectra are presented in Figure 4.12.

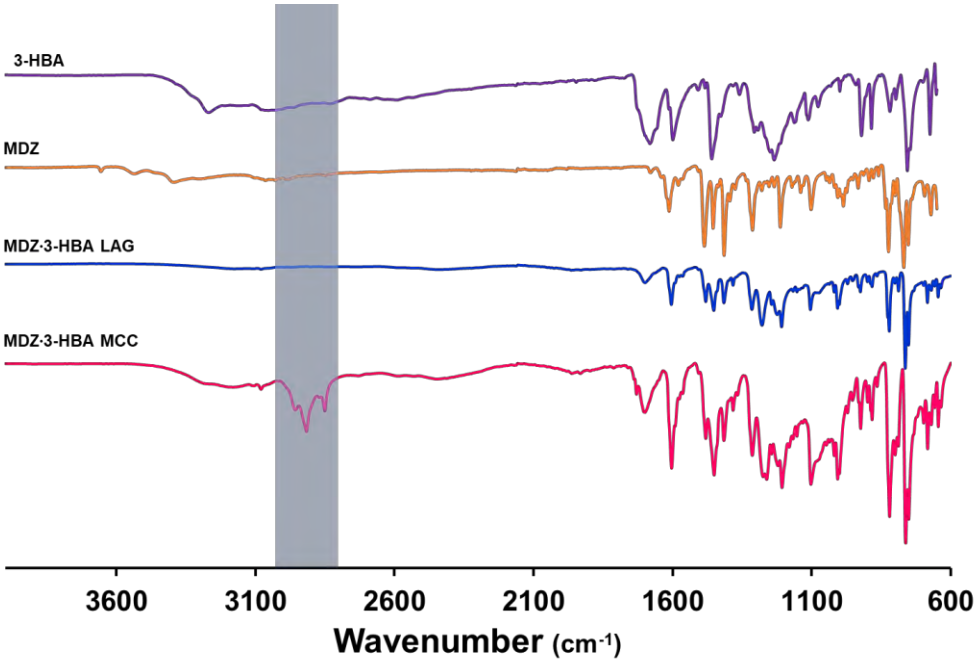

Figure 4.12 – FTIR spectra for 3-HBA, MDZ, MDZ·3-HBA LAG and MDZ·3-HBA MCC.

The spectrum of 3-HBA contains two ν(O-H) stretching bands centred at 3268 cm^{-1} and 3053 cm^{-1}. The band observed at 1682 cm^{-1} is assigned to ν(C=O) while the ν(C-O) and ν(C-OH) bands were assigned to peaks appearing at 1459 cm^{-1} and 1360 cm^{-1}. The MDZ spectrum is mainly characterized by a weak intensity imine band ν(C=N) at 1680 cm^{-1}, an aromatic ν(C=C) band at 1613 cm^{-1} and two aryl halide bands at 1139 cm^{-1} and 770 cm^{-1} for ν(Ar-F) and ν(Ar-Cl), respectively. The MDZ·3-HBA MCC spectrum has multiple peaks in the range 3480-2500 cm^{-1} the most prominent being at 2916 cm^{-1} and 2851 cm^{-1} (highlighted in Figure 4.12). These are attributed to ν(O-H) stretching bands of the 3-HBA and is indicative of hydrogen bonding between MDZ and 3-HBA. The MDZ·3-HBA LAG has two shallow broad bands bands centered at 3210 cm^{-1} and 2406 cm^{-1} that are due to the hydrogen bonding interaction between MDZ and 3-HBA. The spectra for both the MCC and LAG show that the carbonyl stretching bands are shifted from where they occur in pure 3-HBA (see Table 4.7). The carbonyl stretch ν(C=O) at 1682 cm^{-1} shifts to 1699 cm^{-1} and 1697 cm^{-1} due to a O-H···N hydrogen bonding interaction. A new shallow broad band centered at 1948 cm^{-1} in both the LAG and MCC spectra indicates the presence of hydrogen bonding in the structure. Characteristic wavenumbers are reported in Table 4.7.

Table 4.7 – *Vibrational modes for the MDZ·3-HBA MCC, MDZ·3-HBA LAG, MDZ and 3-HBA samples.*

Vibrational Modes	MDZ (cm^{-1})	3-HBA (cm^{-1})	MDZ·3-HBA MCC (cm^{-1})	MDZ·3-HBA LAG (cm^{-1})
ν(O-H)	-	3268-3053	3500-2700	3200-2400
Carboxylic ν(O-H)	-	1360	1366	1382
ν(O-H)	-	-	1948	1948
ν(C=O)	-	1682	1699	1697
ν(C=C)	1613	-	1605	1605
ν(C=N)	1680	-	-	-
ν(Ar-Cl)	770	-	770	-
ν(Ar-F)	1139	-	1139	1145

PXRD patterns for MDZ·3-HBA LAG, MDZ·3-HBA MCC and the starting materials

The PXRD diffractograms of MDZ and 3-HBA are substantially different from those of the LAG, MCC and the calculated diffractograms of the MCC (see Figure 4.13). The LAG, MCC and the calculated diffractograms are very similar to each other. The regions highlited in Figure 4.13 supports this observation. However, there are differences in peak shape and slight shifts in peak position, which could be related to prefered orientation, particle size and also due to differences in the temperatures at which the data were collected. There are also some peaks in the LAG sample that may be evidence of unreacted starting materials. These have been highlighted with asterisks in Figure 4.13. The similarity between the LAG and MCC patterns confirms that the MCC can be prepared under mechanochemical conditions.

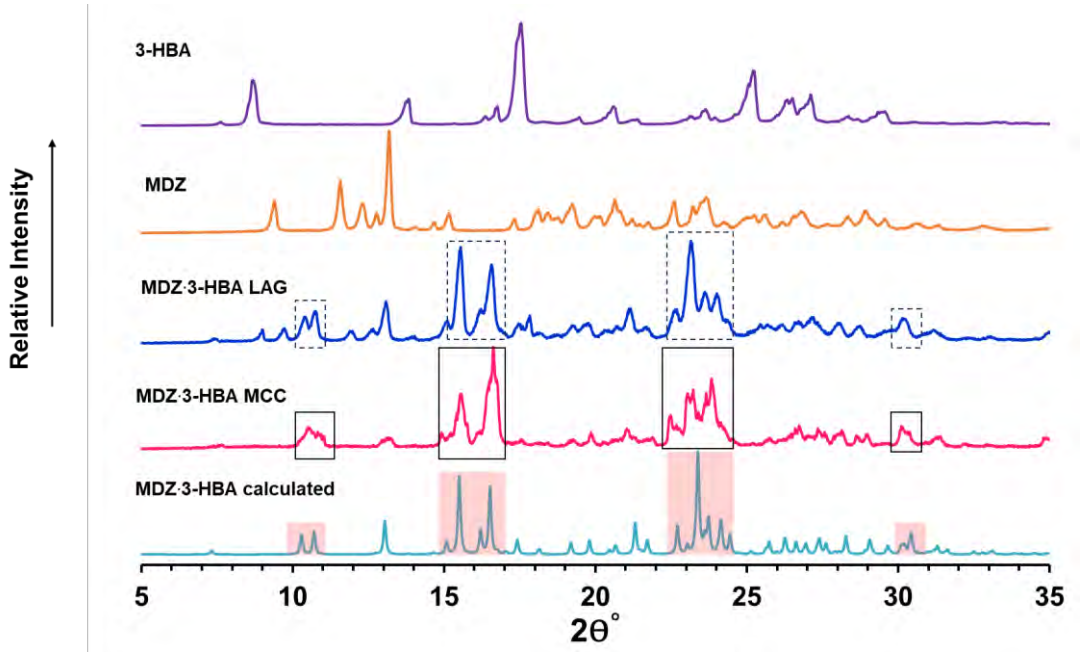

Figure 4.13 – PXRD diffractograms for 3-HBA, MDZ, LAG, MCC and the calculated pattern for MDZ·3-HBA MCC.

Thermal analysis for MDZ·3-HBA MCC, MDZ·3-HBA LAG, MDZ and 3-HBA

The melting range for 3-HBA is between 200.4 – 203.9 °C while MDZ melts in the range 161.6 – 163.7 °C. The MDZ·3-HBA MCC has a single endotherm with an onset temperature of 165.2 °C which is different from MDZ, 3-HBA and the LAG sample (Figure 4.14).

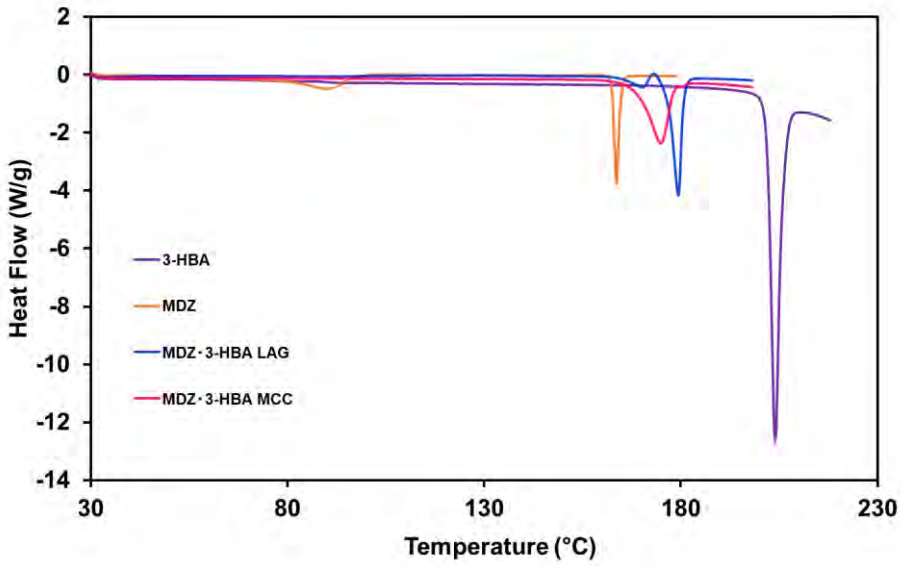

Figure 4.14 — DSC curves of MDZ, 3-HBA, MDZ·3-HBA LAG and MDZ·3-HBA MCC.

The MDZ·3-HBA LAG thermogram contains two endotherms, the first in the range 163.6 – 170.3 °C and a second endotherm in the range 172.7 – 179.4 °C, the first endotherm may be due to unreacted material or a eutectic melt. A temperature cycled experiment was performed on the LAG sample where the LAG sample was heated to just beyond the first endotherm, cooled to ambient temperature and immediately reheated.

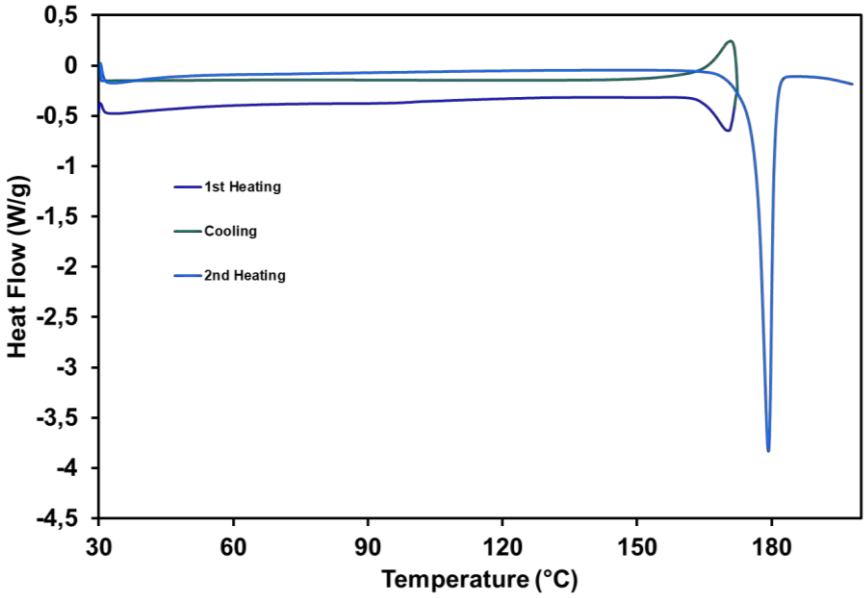

Figure 4.15 – The heat cycled thermogram of MDZ·3-HBA LAG.

However, this time the sample revealed the presence of only a single endotherm in the range 168.8 – 179.3 °C as depicted in Figure 4.15. This is consistent with evidence for unreacted material from the PXRD patterns. All onset and peak melt temperatures are reported in Table 4.8.

Table 4.8 – Melt onset and peak temperatures of starting materials, LAG, and MDZ·3-HBA MCC.

Sample	T_{onset} (°C)	T_{peak} (°C)
MDZ	161.6	163.7
3-HBA	200.4	203.9
MDZ·3-HBA LAG 1st heating	163.6	170.3
MDZ·3-HBA LAG	172.7	179.4
MDZ·3-HBA LAG 2nd heating	168.8	179.3
MDZ·3-HBA MCC	165.2	174.8

4.3 MDZ·PABA MCC

4.3.1 Introduction

The MDZ·PABA LAG was prepared by grinding equimolar quantities of MDZ (0.49 mmol, 160 mg) and PABA (0.49 mmol, 67 mg) using a mortar and pestle. 10 µl of methanol were added after grinding for 5 minutes, followed by an additional 10 minutes of grinding.

Single-crystal X-ray analysis of MDZ·PABA MCC

The crystals were prepared by dissolving the MDZ·PABA LAG powder (8 mg) in 8 ml of diethyl ether. The solvent was added gradually whilst gently heating the solution to 25 °C to ensure that the solute was fully dissolved. The solution was filtered through a 0.45 µm nylon syringe filter into a vial and covered with a vial lid with a single hole to slow down evaporation. The solution was left to evaporate slowly under ambient conditions. A suitable single crystal was chosen for SCXRD characterization.

Data collection and space group determination

A Bruker D8 Venture diffractometer was utilized to collect single-crystal data for each crystal. The unit cell parameters, crystal system, and space group of each crystal are determined using X-ray diffraction data. A preliminary unit cell dimension check reveals that the MDZ·PABA MCC crystallizes in the monoclinic space group $P2_1/c$.

Structure solution and refinement

Structure solution was completed using SHELXT[1] and SHELXL[2] was used for the refinement of the MDZ·PABA MCC. Based on well-behaved isotropic temperature factors, all atoms were refined anisotropically, and hydrogen atoms were placed in idealized positions in a riding model. Peaks from a difference Fourier map were used to refine hydrogen atoms for heteroatoms. The data collection and refine parameters are summarized in Table 4.9.

Table 4.9 – Data-collection and refinement parameters for MDZ·PABA MCC.

Data-collection and refinement parameters	
Formula unit	$(C_{18}H_{13}ClFN_3)(C_7H_7NO_2)$
Formula mass (g mol^{-1})	462.90
Crystal system	Monoclinic
Space group	$P2_1/c$ (No. 14)
a/Å	37.0216(15)
b/Å	8.0012(2)
c/Å	15.4552(6)
α/°	90
β/°	102.0340(10)
γ/°	90
Volume (Å^3)	4477.5(3)
Z	8
D_{calc} (g cm^{-3})	1.373
F (000)	1920
μ (MoKα) (mm^{-1})	0.210
Crystal size (mm^3)	0.13 × 0.14 × 0.33
Temperature (K)	100(2)
Range scanned θ (°)	2.25 – 26.4
Index ranges	-46: 46; -10: 10; -19: 19
Total number of reflections collected	193388
Number of unique reflections	9127
Number of reflections with $I > 2\sigma(I)$	6542
Number of least-square parameters	624
R_{int}	0.173
S	1.04
R_1 (I>2σ (I))	0.0789
wR_2	0.2237
Weighting scheme parameters	a = 0.1488, b = 2.6719
$(\Delta/\sigma)_{mean}$	0.00
Δρ excursions (e Å^{-3})	-0.46, 1.80

Molecular structure and noncovalent interactions

The asymmetric unit of MDZ·PABA consists of two molecules of MDZ and two molecules of PABA, Figure 4.16 (A). Each MDZ molecule is directly hydrogen bonded to one PABA molecule through an O-H···N interaction, where the hydroxyl moiety of PABA hydrogen bonds

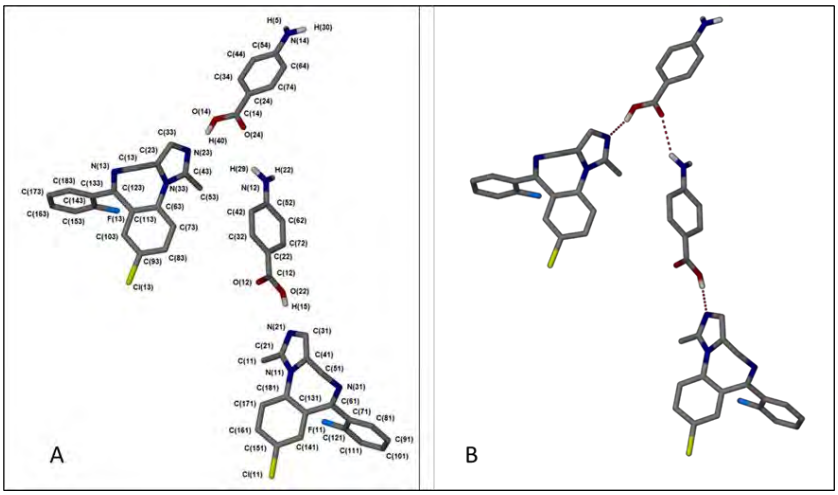

Figure 4.16 – Labelled asymmetric unit of the MDZ·PABA MCC and (B) – the hydrogen bonded asymmetric unit of the MDZ·PABA MCC.

to one of the nitrogen atoms of the imidazole ring of MDZ (O(22)-H(15)···N(21) and O(14)-H(40)···N(23)), Figure 4.16 (B). The two PABA molecules are, in turn, hydrogen bonded to each other via a single N-H···O interactions (N(12)-H(29)···O(24)). MDZ and PABA molecules which hydrogen bond directly to each other are coloured coded and depicted in Figure 4.17.

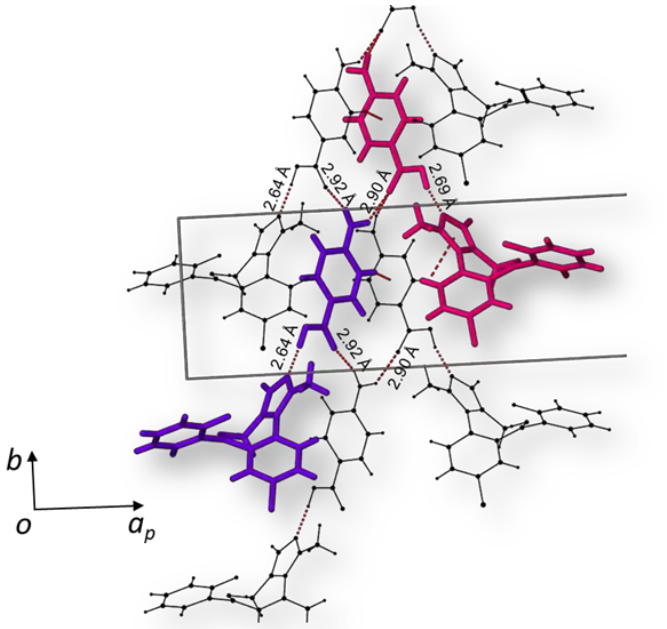

Figure 4.17 – View down the c axis showing some of the noncovalent interactions in the structure.

There are also several C-H···π and a single N-H···π interactions in the structure. These occur between the PABA molecules as in the case of N(14)-H(30)···[C22-C32-C42-C52-C62-C72] and between PABA and MDZ molecules such as C(34)-H(34)···[N23-C33-C23-N33-C43]. Some of the noncovalent interactions have been depicted in Figure 4.17. The most pertinent noncovalent interactions are reported in Table 4.10.

Table 4.10 – Noncovalent interactions for MDZ·PABA MCC.

D-H···A	D···A (Å)	D-H···A (°)	Symmetry Code
N14-H5···$O24	2.921(4)	158(3)	x,1+y,z
O22-H15···N21	2.688(4)	157(2)	.
N12-H22···O12	2.903(4)	159(3)	x,1+y,z
N12-H29···O24	3.220(4)	144(4)	-
O14-H40···N23	2.637(4)	165(6)	-
C13-H13B···F13	3.343(4)	148.0	x,1/2-y,-1/2+z
C51-H51A···F11	3.269(4)	159.0	x,-3/2-y,-1/2+z
C62-H62···O12	3.247(4)	132.0	x,1+y,z
C161-H161···O12	3.343(5)	139.0	x,-1/2-y,-1/2+z
N14-H30···[C22-C72]	3.291(3)	149(2)	x,5/2-y,1/2+z
C34-H34···[N23-C43]	3.631(3)	129.0	x,1+y,z
C42-H42···[C24-C74]	3.458(4)	147.0	x,-1+y,z
C72-H72···[N11-C41]	3.582(4)	131.0	x,1+y,z
C91-H91···[N11-C41]	3.474(4)	131.0	2-x,-1/2+y,1/2-z
C173-H173···[N23-C43]	3.430(4)	131.0	1-x,-1/2+y,1/2-z

[C22-C72], [N23-C43], [C24-C74], [N11-C41], [N11-C41] and [N23-C43] are rings.

Crystal Packing

The MDZ·PABA MCC units stack in symmetry related pairs forming columns that are parallel to the *c* axis. These colour coded columns alternate along the *a* axis with layers of PABA molecules located between the columns of MDZ molecules as depcited in Figure 4.18.

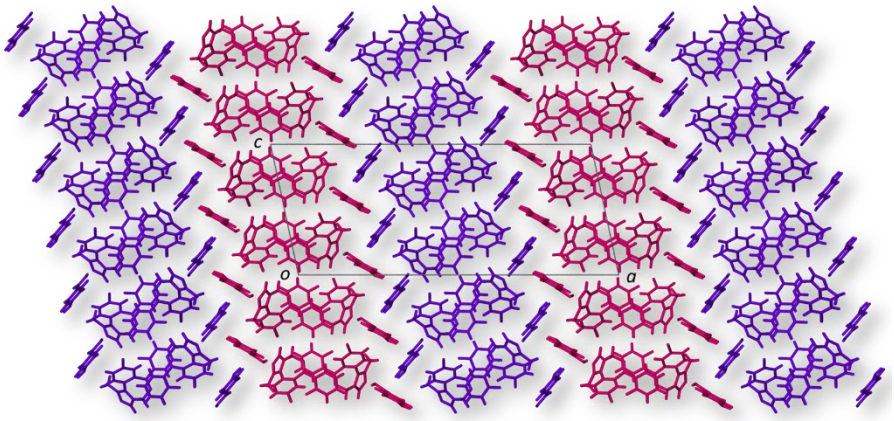

Figure 4.18 – View of the MDZ·PABA MCC packing arrangement down the b axis showing the alternating columns.

The columns of MDZ molecules are directly hydrogen bonded to the PABA molecules that form the layers between the colums as mentioned prevously. The view down the *c* axis clearly shows the symmetry related pairs of MDZ molecules (pink or purple), which stack parallel to *c* and along the *a* axis, as depicted in Figure 4.19.

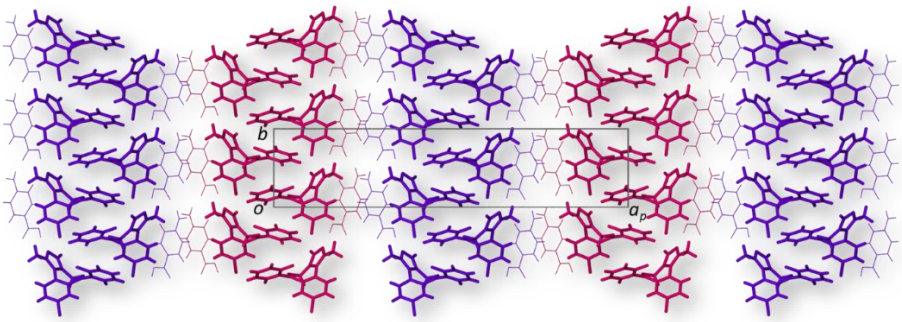

Figure 4.19 – View down the c axis showing columns of MDZ molecules interleaved by layers of PABA molecules.

4.3.2 Bulk characterization

FTIR spectra of MDZ·PABA LAG sample, starting and crystalline materials

The individual starting materials along with the milled and recrystallised materials were characterised using FTIR spectroscopy. The spectra of the starting materials were used as a reference for identifying new phase formation. These spectra, along with those of the LAG sample and the bulk crystalline material, are presented in Figure 4.20. The FTIR spectrum of PABA displays stretching bands at 3460 cm^{-1} and 3360 cm^{-1} which are assigned to ν(O-H) and ν(N-H), respectively. There is also a broad ν(O-H) stretching band that occurs in the range

3231-2548 cm^{-1} due to the hydrogen bonding in PABA. The ν(C=O) and ν(C-OH) characteristic peaks occur at 1661 cm^{-1} and 1172 cm^{-1} whilst the ν(C-N) band is assigned to 1286 cm^{-} in the PABA spectrum. The spectra observed are well supported by evidence from the literature.[6] The MDZ spectrum is mainly characterized by a weak intensity imine band ν(C=N) at 1680 cm^{-1}, an aromatic ν(C=C) band at 1613 cm^{-1} and two aryl halide bands ν(Ar-F) at 1139 cm^{-1} and ν(Ar-Cl) at 770 cm^{-1}.

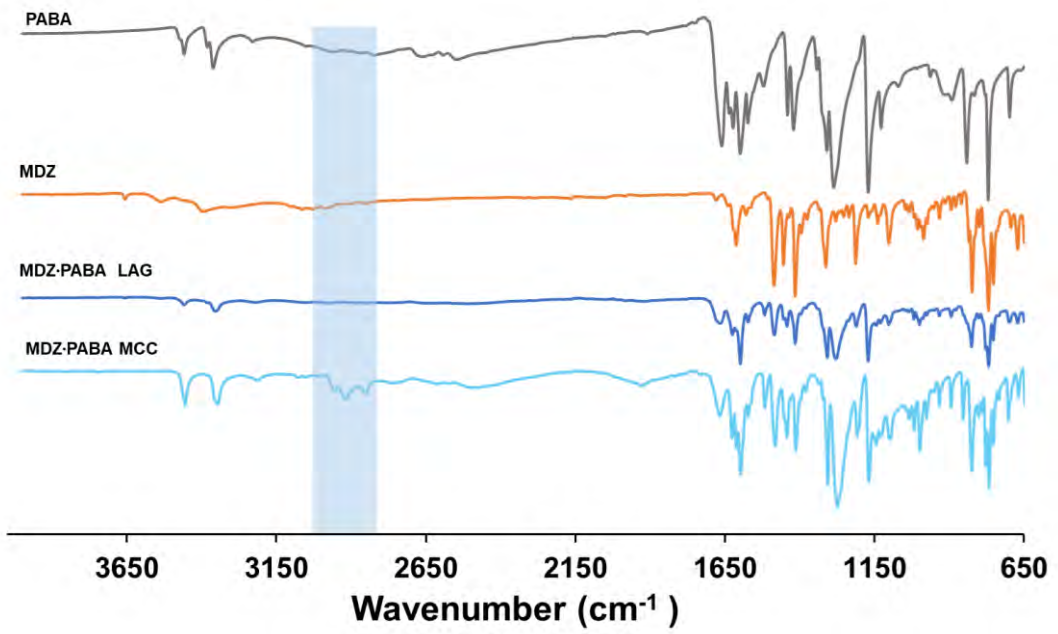

Figure 4.20 – FTIR spectra of PABA, MDZ, MDZ·PABA LAG and MCC.

The MDZ·PABA MCC and LAG spectra display two stretching bands at 3457 cm^{-1} and 3348 cm^{-1}, corresponding to ν(O-H) and ν(N-H) respectively. In both the MCC and LAG spectra, the amino, carbonyl, and hydroxyl stretching bands are shifted compared to their positions in pure PABA (Table 4.11). The MCC spectrum features a broad band (highlighted in Figure 4.20) in the range of 2977-2788 cm^{-1}, with three weak stretching bands at 2969 cm^{-1}, 2916 cm^{-1}, and 2854 cm^{-1}. This is attributed to PABA and is indicative of hydrogen bonding between MDZ and PABA. The carbonyl stretch ν(C=O) shifts from 1662 cm^{-1} to 1669 cm^{-1}, possibly due to a O-H···N hydrogen bonding interaction. Additionally, a new shallow broad band centred at 1928 cm^{-1} in the MCC spectrum, indicates hydrogen bonding within the structure. A summary of the characteristic wavenumbers is provided in Table 4.11.

Table 4.11 – Vibrational modes for the MDZ·PABA MCC, MDZ·PABA LAG, MDZ and PABA samples.

Vibrational modes	MDZ (cm^{-1})	PABA (cm^{-1})	MDZ·PABA LAG (cm^{-1})	MDZ·PABA (cm^{-1})
ν(O-H)	-	3460	3457	3457
Carboxylic ν(O-H)	-	1172	1172	1169
ν(O-H)	-	-	1927	1927
ν(C=O)	-	1662	1669	1669
ν(C-N)	-	1288	1277	1275
ν(N-H)	-	3360	3348	3348
ν(C=N)	1680	-	-	-
ν(C=C)	1613	-	-	-
ν(Ar-Cl)	770	-	-	-
ν(Ar-F)	1139	-	-	-

Powder patterns of MDZ·PABA LAG sample, starting and crystalline materials

The PXRD diffractograms of MDZ and PABA differ significantly from those of the LAG, MCC, and the calculated diffractograms of the MCC (refer to Figure 4.21). In contrast, the LAG, MCC, and calculated diffractograms are quite similar to each other. The highlighted regions in Figure 4.21 support this observation. However, differences in peak shape and slight shifts in peak position are noted, potentially due to preferred orientation, particle size, and varying temperatures at which the data were collected. The similarity between the LAG and MCC patterns confirms that the MCC can be synthesized under mechanochemical conditions.

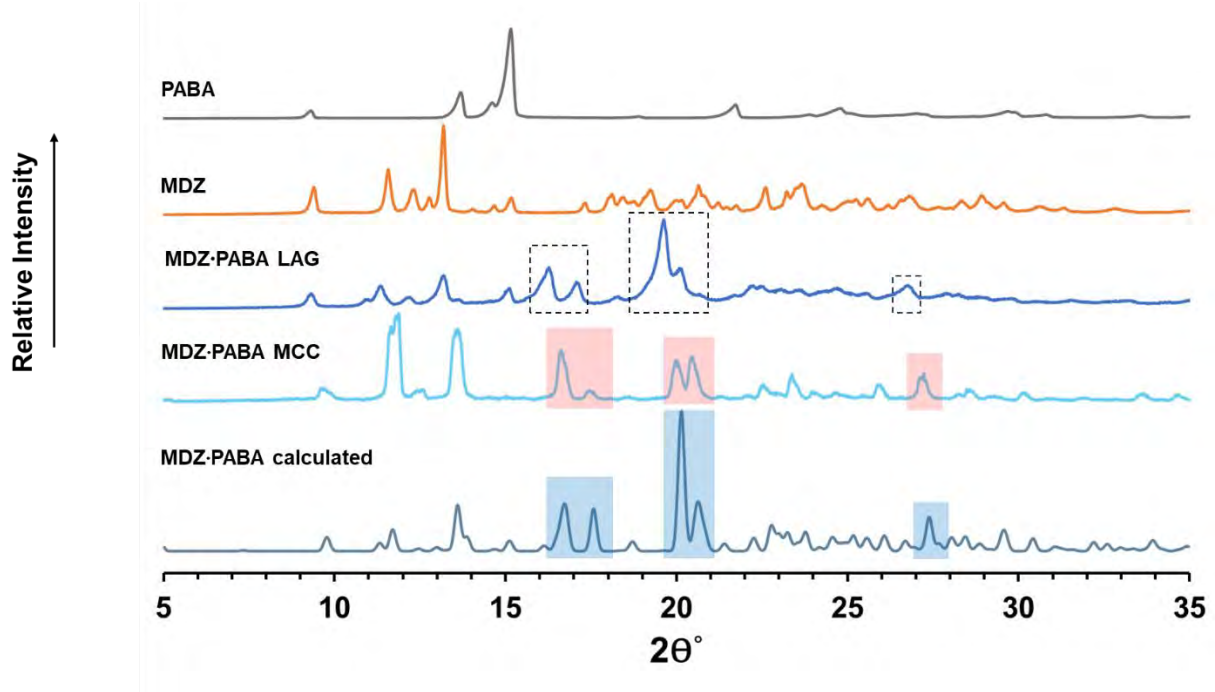

Figure 4.21 – Powder patterns for the starting materials, LAG, experimental and calculated pattern for MDZ·PABA MCC.

Thermal analysis for MDZ·PABA MCC. MDZ·PABA LAG, MDZ and PABA

The melting point range for PABA is 186.8 – 190.3 °C and that of MDZ is 161.6 – 163.7 °C, Figure 4.22. The melting point range for MDZ·PABA LAG is 162.9 – 170.8 °C this is indicative of a new phase or at least co-crystal formation. It turns out that this range coincides with the melting range of the single crystals of the MDZ·PABA MCC, which has a single endotherm with a peak temperature of 172.4 °C.

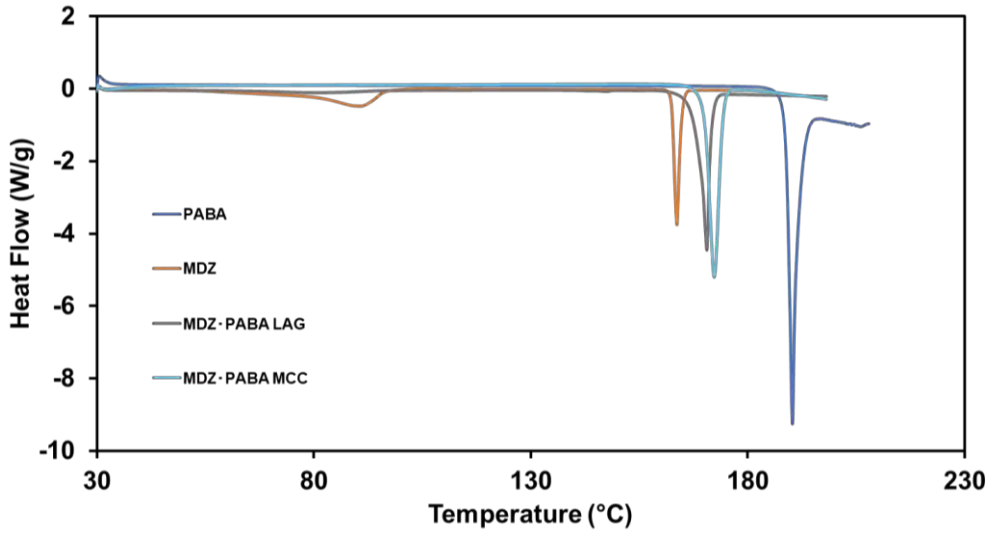

Figure 4.22 – DSC heating curves of PABA, MDZ, MDZ·PABA LAG and MDZ·PABA MCC.

In Table 4.12 a summary of all the onset and peak temperatures of the starting materials, ground samples, and co-crystals is provided.

Table 4.12 – Melt onset and peak temperatures of starting materials, LAG, and salt for MDZ·PABA.

Sample	T_{onset} (°C)	T_{peak} (°C)
MDZ	161.6	163.7
PABA	186.8	190.3
MDZ·PABA LAG	162.9	170.8
MDZ·PABA MCC	167.3	172.4

4.4 Summary

Through our attempts of making co-crystals of MDZ with different coformers, we successfully isolated and fully characterized three multicomponent co-crystals: MDZ·BA, MDZ·3-HBA and MDZ·PABA. These were all prepared using mechanochemistry and slow evaporation techniques. After an extensive search in the CSD[3], we found that none of these co-crystals have previously been reported.

4.5 References

1 Sheldrick G.M. SHELXT - Integrated Space-Group and Crystal-Structure Determination. *Acta Crystallogr A.,* **2015**, *71* (1), 3–8.

2 Sheldrick G. M. Crystal Structure Refinement with SHELXL. *Acta Crystallogr C Struct Chem.,* **2015**, *71*, 3–8.

3 Ferrence G.M., Tovec C.A., Holgate S.J.W., Johnson N.T., Lightfoot M.P., Nowakowska-Orzechowska K.L., Ward S.C., CSD Communications of the Cambridge Structural Database, *IUCrJ.*, **2023**, 10, 6-15.

4 Guan X-H., Guang-Hao C. and Chii S., ATR-FTIR and XPS study on the structure of complexes formed upon the adsorption of simple organic acids on aluminium hydroxide, *J. Environ. Sci.,* **2007**,19, 438-443.

5 Zhou Z., Chan H.M., Sung H.H.Y., Tong H.H.Y., and Zheng Y., Identification of new cocrystal systems with stoichiometric diversity of salicylic acid using thermal methods. *Pharm. Res.*, **2016**, 33, 1030–1039.

6 Anandhi S., Rajalakshmi M., Shyju T.S., and Gopalakrishnan R., Growth and characterization of an adduct 4-aminobenzoic acid with nicotinic acid. *J. Cryst. Growth.*, **2011**,318,774–779.

Chapter 5: Conclusions

The research reported covers the meticulous preparation of five novel multicomponent crystals of the benzodiazepine, midazolam and carboxylic acid coformers that are structural analogues of methyl paraben were characterised using FTIR, DSC, TGA and PXRD. The multicomponent crystals formed were established as three co-crystals and two salts. The molecular structure of each of these was elucidated using single-crystal X-ray diffraction.

5.1 Crystal preparation and characterization

The multicomponent crystals were successfully prepared using mechanochemical and solvent recrystallization methods. The mechanochemical approaches used included neat grinding and liquid assisted grinding with methanol and water as solvents to produce the ground powders. Single crystals were produced using a slow solvent evaporation technique from diethyl ether.

5.2 Midazolam Multicomponent crystals

Through the use of midazolam hydrochloride salt and its subsequent transformation into midazolam free base, we demonstrated a robust method for producing high-purity crystalline forms under ambient conditions (22 °C, 101.3 kPa). The use of liquid assisted grinding with coformers such as MP, SA, BA and 3-HBA resulted in the formation of multicomponent crystals, each characterized by unique structural and thermal properties.

WPRU1 is a commercial product that demonstrated instability by forming an insoluble crystal in solution. This crystal formation may be related to the manufacturing process. Using mechanochemistry, we successfully synthesized WPRU1 in the solid phase (WPRU1 LAG), as confirmed by the PXRD diffractograms. A particularly noteworthy finding was the identification and characterization of the WPRU1 MCC, which revealed a complex hydrogen bonded network formed between MDZ·HCl, MDZ free base and MP. The two MDZ molecules interact through an N-H···N hydrogen bond, connecting both molecules via their imidazole groups, while MP hydrogen bonds with the chloride ion via the hydroxyl group.

5.2.1 Noncovalent interactions

In this study, the coformers were selected based on two key features; 1) they are structural analogues of MP, and 2) all coformers contain carboxylic acid functional groups. Carboxylic acids are known for their propensity for establishing noncovalent interactions and MP due to the information provided by our industrial partner.

MDZ and SA interact through a charge assisted $N\text{-}H^{+}\cdots O^{-}$ hydrogen bond, involving the protonated nitrogen atom in the imidazole ring of MDZ and the deprotonated oxygen atom of the carboxylate moiety of SA. The prevalent hydrogen bond for the remaining coformer-MDZ

interaction is the O-H···N contact, where MDZ as the hydrogen bond acceptor molecule interacts via the nitrogen atom of an imidazole ring to the hydroxyl moiety of the coformer carboxylic acid (hydrogen bond donor), as in the case of BA, 3-HBA, and PABA. It is noteworthy that PABA contains both NH_2 and COOH functional groups, which is indicative of an interaction preference that is likely because the oxygen atom of the hydroxyl moiety being more electronegative than the nitrogen atom of the amine functional group, which may make it a more favourable site for hydrogen bonding.[1]

5.2.2 Mechanochemistry

Mechanochemistry proved to be the most effective method for preparing MCC, as solvent-based methods without prior grinding or milling did not result in co-crystal formation. Liquid assisted grinding emerged as the optimum approach for preparation of the MCC especially since only small volumes of solvent of between 0.05 and 0.15 ml were added. LAG enhances material mobility, thereby increasing the likelihood of co-crystal formation. Other advantages of LAG are that the approach aligns with the principles of green chemistry and sustainability, particualry in respect of waste reduction, elimnation of harzardous synthetic procedures, improved energy efficiency, amonsgt others.[2] As a direct comparison to solution based methods mechanochemistry faciliates product identification and charaterisation as long waiting times for precipitation from solution, are avoided.

5.2.3 Physicochemical properties

The multicomponent crystals exhibit enhanced thermal stability when compared to MDZ free base; however, further analyses are required to determine whether the solubility, chemical stabiliity and other critical performace parameters including clinical efficacy have been altered in any way.

5.3 Other combinations

A list of additional combination crystals and salts that were successfully prepared as part of this work is summarised in Table 5.1 and 5.2. Due to time constraints a comprehensive description of these is not included in this dissertation.

Table 5.3 – Additional combination crystals investigated during the course of this work.

Combinations	Synthesis method		
	NG	LAG (MeOH)	LAG (ethyl acetate)
MDZ + 4-HBA	✓	✓	✓
MDZ + 3,4-DHBA	✓	✓	✓
MDZ + PAS	✓	-	-
MDZ + Isonicotinic acid	✓	-	-
Bromazepam + 3-HBA	✓	✓	✓
Bromazepam +4-HBA	✓	✓	✓
Bromazepam + 3,4-DHBA	✓	✓	✓
Bromazepam + PAS	✓	✓	-
Bromazepam + Isonicotinic acid	✓	✓	-

Table 5.2 – Additional salts investigated during the course of this work.

Salts	Slow evaporation solvent		
	Water	Methanol	Ethanol
Anhydrous Midazolam HCl	-	✓	-
Midazolam HCl dihydrate ($MDZ{\cdot}HCl{\cdot}2H_2O$)	-	-	✓
Midazolam HCl quasiquihydrate $2(MDZ{\cdot}HCl{\cdot}1.5H_2O)$	✓	-	-

5.4 Suggestions for future work and closing remarks

Looking ahead, several potential areas of investigation emerge from these data and require further attention. There is a need to characterize the MDZ MCC using DOSY NMR and to undertake permeability, solubility, chemical stability, and dissolution rate studies. These additional analyses will provide an opportunity for the assessment of the physicochemical behaviour of the MCC. Several of the LAG samples showed evidence of the presence of unreacted starting materials, which suggest that the preparation conditions require deeper exploration. It would be advantageous, from an efficiency and cost perspective, to use statistical approaches such as design of experiments (DoE) methodology to determine the optimum conditions for preparation. Critical parameters that may need to be investigated include but are not limited the volume and type of solvent used, weight of solid reactants used, milling frequency, milling time and number of milling media used as well as temperature.

In conclusion, this dissertation highlights the transformative potential of multicomponent crystal engineering in the pharmaceutical industry. Developing novel crystalline forms of

midazolam, has laid down groundwork for future innovations in design, preparation and formulation of potentially useful combination products. Pharmaceutical dosage forms such as suspensions and solutions containing preservatives can exhibit stability problems due to the formation of crystalline precipitates. It is essential to assess the potential for this occurrence during the formulation development of MDZ and other benzodiazepines. A critical factor to consider is the required dose per ml in relation to the solubility of the API, which is what initiated this research. As crystal engineering continues to evolve, many of the insights gained from this work provide a valuable foundation in the development of potential tranquilizer pharmaceuticals for veterinary use.

5.5 References

1 Böhm H.-J., Brode S., Hesse U., and Klebe G., Oxygen and Nitrogen in Competitive Situations: Which is the Hydrogen-Bond Acceptor? *Chem. Eur. J.*, **1996**, 2(12), 1509-1513

2 Anastas P.T., Warner J.C., *Green Chemistry: Theory and Practice*, Oxford University Press, New York, **1985**.

Appendix

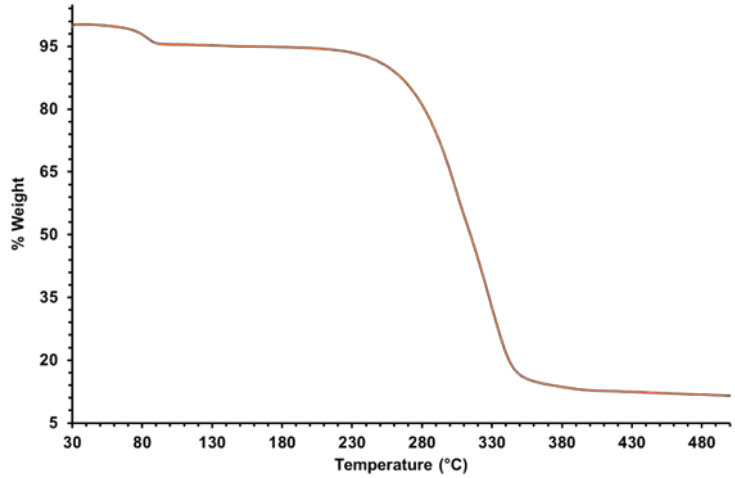

Figure 1 – TGA thermogram for MDZ

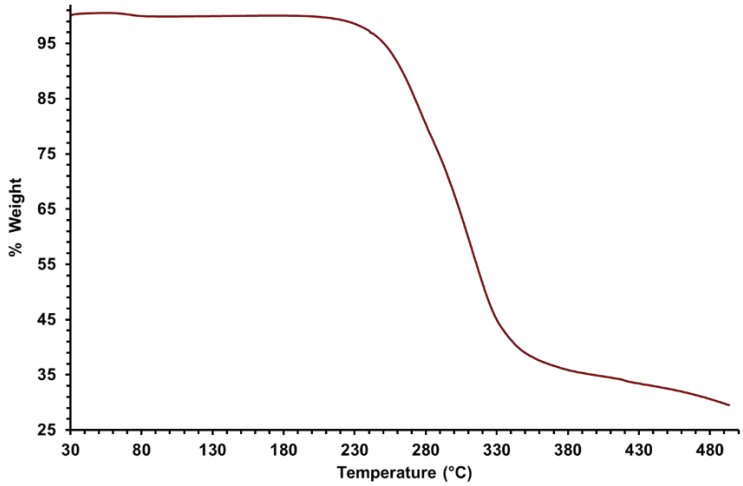

Figure 2 – TGA thermogram for MDZ HCl

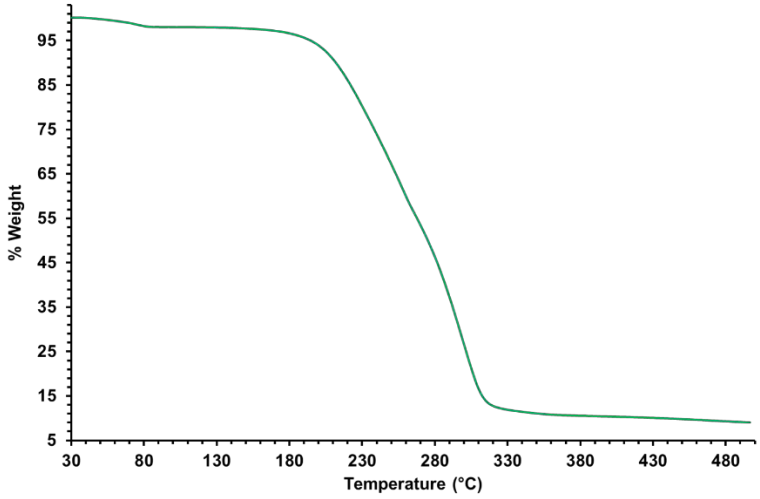

Figure 3 – TGA thermogram for MDZ·BA LAG

Bulk characterization data for all structures

https://drive.google.com/drive/folders/1fIfDTQZu8fuJYuoRJUbqDAkTu_u7Ghl7?usp=sharing

Additional files (.sup files) for all crystallographic structures

https://drive.google.com/drive/folders/1XzyqX43D1lLB96qdT2Hc8BxGWY5ejTxm?usp=sharing